Satellite-based modeling of wetland methane emissions on a global scale (SatWetCH4 1.0)

Juliette Bernard[1,2], Elodie Salmon[1], Marielle Saunois[1], Shushi Peng[3], Penélope Serrano-Ortiz[4], Antoine Berchet[1], Palingamoorthy Gnanamoorthy[5,6], Joachim Jansen[7], and Philippe Ciais[1]

[1]Laboratoire des Sciences du Climat et de l'Environnement, CEA-CNRS-UVSQ, Gif-sur-Yvette, France
[2]LERMA, Paris Observatory, CNRS, PSL, Paris, France
[3]College of Urban and Environmental Sciences, Peking University, Beijing 100871, China
[4]Department of Ecology, Andalusian Institute for Earth System Research (CEAMA-IISTA), University of Granada, Spain
[5]CAS Key Laboratory of Tropical Forest Ecology, Xishuangbanna Tropical Botanical Garden, Chinese Academy of Sciences, Menglun, China
[6]Coastal Systems Research, M. S. Swaminathan Research Foundation, Chennai, India
[7]Department of Ecology and Genetics/Limnology, Uppsala University, Uppsala, Sweden

Correspondence: Juliette Bernard (juliette.bernard@obspm.fr)

Abstract. Wetlands are major contributors to global methane emissions. However, their budget and temporal variability remain subject to large uncertainties. This study develops the Satellite-based Wetland CH_4 model (SatWetCH4), which simulates global wetland methane emissions at 0.25°x0.25° and monthly temporal resolution, relying mainly on remote sensing products. In particular, a new approach is derived to assess the substrate availability, based on Moderate-Resolution Imaging Spectroradiometer data. The model is calibrated using eddy covariance flux data from 58 sites, allowing for independence from other estimates. At the site level, the model effectively reproduces the magnitude and seasonality of the fluxes in the boreal and temperate regions, but shows limitations in capturing the seasonality of tropical sites. Despite its simplicity, the model provides global simulations over decades and produces consistent spatial patterns and seasonal variations comparable to more complex Land Surface Models. Such an independent data-driven approach based on remote-sensing products is intended to allow future studies of intra-annual variations in wetland methane emissions. In addition, our study highlights uncertainties and issues in wetland extent datasets and the need for new seamless satellite-based wetland extent products. In the future, there is potential to integrate this one-step model into atmospheric inversion frameworks, thereby allowing optimization of the model parameters using atmospheric methane concentrations as constraints, and hopefully better estimates of wetland emissions.

1 Introduction

The article 1.1 of the Ramsar Convention (1971) defines wetlands as "areas of marsh, fen, peatland, or water, whether natural or artificial, permanent or temporary, with water that is static or flowing, fresh, brackish, or salt, including marine water areas the depth of which at low tide does not exceed six meters". Each wetland exhibits very specific local conditions, such as water source (ombrotrophic or minerotrophic source) and quantity (groundwater level, soil moisture), vegetation (types, density), and

soil properties (pH, carbon content, microbial communities). These areas harbor a rich biodiversity of flora and fauna and play

20 a significant role in regulating water resources, water purification, and flood prevention (Denny, 1994; Meli et al., 2014).

Wetlands are also a crucial element for climate. On the one hand, waterlogged conditions in wetlands lead to a reduction in the rate of decomposition of soil organic carbon (SOC) and thus to a significant accumulation of carbon, such as in peatlands. This wetland SOC stock has been estimated at around 520 to 710 PgC worldwide (Poulter et al., 2021). On the other hand, anaerobic conditions favor the production of methane (Torres-Alvarado et al., 2005), a powerful greenhouse gas with a global

25 warming potential of 80 $\pm$26 over 20 years (IPCC 2021 AR6 Chap.7, Table 7.15). In the last Global Methane Budget (GMB) (Saunois et al., 2020), it has been estimated that methane emissions from wetlands contribute for approximately 12 to 36% of the total methane sources. These estimates have been established from bottom-up (102-182 Tg CH_4 yr^{-1}, 12-31% of total annual sources) and top-down approaches (159-200 Tg CH_4 yr^{-1}, 27-36% of total annual sources).

Top-down approaches rely on a prior estimate of the ensemble of methane fluxes, including prior knowledge of wetland

30 emissions, and are therefore dependent on bottom-up estimates. Bottom-up approaches estimate methane fluxes from wetlands using formulations ranging from the simplest to the most complex, such as in Land Surface Models (LSMs). LSMs represent the budgets of water, energy, and carbon under some meteorological constraints. They account for soil processes in a series of successive steps that explicitly simulate part or all of the following processes: methane production, oxidation, and transport by diffusion, ebullition or higher plants (Riley et al., 2011; Morel et al., 2019; Salmon et al., 2022).

35 In the context of climate change, understanding past and predicting future trends in global wetland methane emissions are key issues, but these trends are still uncertain (Jackson et al., 2020). Although they try to represent complex pathways involved in methane emissions, LSMs models still lead to significant uncertainties in terms of global total emissions, seasonal cycle and spatial patterns (Melton et al., 2013; Saunois et al., 2020). In particular, the internal wetland surface area varies considerably from one LSM to another (Melton et al., 2013). Moreover, a large part of the studies (Zhu et al., 2013; Bohn et al., 2015;

40 Guimberteau et al., 2018; Peltola et al., 2019; Qiu et al., 2019; Salmon et al., 2022; Tenkanen et al., 2021; Kuhn et al., 2021; Rößger et al., 2022) focus only on boreal and temperate regions. In fact, the boreal regions are of great interest because temperatures there are rising faster than the global average (England et al., 2021; Post et al., 2019; Previdi et al., 2021) and permafrost is thawing, which could lead to large increases in carbon dioxide and methane emissions (Schuur et al., 2022). However, about three quarters of global wetland methane emissions actually occur in tropical regions (Saunois et al., 2020),

45 where wetland methane emissions are still poorly understood (Meng et al., 2015), partly due to the scarcity of measurements in tropical wetlands compared to boreal and temperate regions (Delwiche et al., 2021).

Simpler formulations than LSMs, operating on a global scale (Gedney, 2004; Bloom et al., 2017; Albuhaisi et al., 2023) implicitly represent soil processes in a one-step approach between soil organic carbon content, which is the main substrate for methanogenesis, and CH_4 emissions. While these models may not provide greater accuracy compared to LSMs, they have the

50 advantage of operating faster (within a few seconds) and relying on only a few parameters and variables. They provide quick estimates and can be valuable for sensitivity testing or trend analysis. Typically, the variables considered in the different models are the wetland area, the soil temperature, a proxy for carbon substrate and sometimes a local water variable (water table depth,

WTD, or soil water content, SWC). The differences between these simple models depend on the equation formulation, the choice of data sets used to constrain the variables and the calibration method.

55   Methanogenic bacteria use organic carbon from litterfall, root exudates, dead plants and dissolved organic carbon that has already been broken down to low molecular weight molecules by other microorganisms (Nzotungicimpaye et al., 2021; Torres-Alvarado et al., 2005; Bridgham et al., 2013). Quantifying the organic matter available for methanogenesis is not trivial, as it cannot be measured directly. Many proxies are used in the literature without a consensus being found (Wania et al., 2013; Melton et al., 2013): Some models use NPP as a proxy (e.g. UW-Vic, Walter and Heimann (2000)), while others consider

60   that methane production could be derived by multiplying heterotrophic respiration by a CO_2:CH_4 ratio (e.g. LPJ, CLM4Me, SDGVM). Other models use SOC as a proxy for carbon available for methanogenesis (Gedney, 2004). However, not all SOC can be used for respiration by methanogenic bacteria. Carbon pool models are embedded in some LSMs such as ORCHIDEE (Ringeval et al., 2010; Salmon et al., 2022) to distinguish readily available SOC from recalcitrant SOC.

In the absence of global data on substrate availability, Gedney (2004) proposed a simple equation based on wetland fraction,
65   temperature, and total soil carbon. These three variables were modelled using the Met Office climate model (Gordon et al., 2000) coupled to the land surface scheme MOSES-LSH (Gedney and Cox, 2003), and their model was run for the period 1990-1998. Bloom et al. (2017) also used a simplified approach based on an equation relying on wetland fraction, soil temperature, soil heterotrophic respiration, and fed with different datasets, forming the WetCHARTs 1.0 ensemble for 2001-2015. The heterotrophic respiration data were derived by terrestrial biosphere models. In general, the proxies used in these studies are
70   derived from models (LSMs, hydrological models...) and in some rare cases from remote sensing data. Recently, Albuhaisi et al. (2023) proposed a methane emission formulation fed only by satellite and satellite-derived data sets for soil moisture and SOC. However, this approach was carried out only in the boreal region for the period 2015-2021.

The calibration methods of these approaches have varied in recent years due to important changes in the available data. The first attempt by Gedney (2004) assumed that the global atmospheric concentration anomalies were solely due to wetlands.
75   This approximation is highly questionable according to current estimates of anthropogenic and natural methane emission trends (Jackson et al., 2020). Too few flux data measurements were available in the early 2000s to be used for calibration. In WetCHARTs (Bloom et al., 2017), the model calibration was performed by constraining total wetland methane emissions to the GMB ensemble mean (Saunois et al., 2016), and as such was not independent of other LSM approaches. However, recent efforts by the FLUXNET community (Delwiche et al., 2021) have led to the construction of a unified database of methane
80   fluxes measured by eddy covariance worldwide, offering the possibility of new independent calibration methods. The eddy covariance method provides stable and continuous in situ flux measurements over relatively large areas (>100m^2) with limited environmental disturbance (Baldocchi et al., 2001; Kumar et al., 2017). The FLUXNET-CH4 database includes some ancillary data such as soil temperature, gross primary productivity, WTD or SWC, but not for all sites. An important issue is still the inhomogeneous distribution of flux towers across the globe, with sites mainly located in temperate and boreal regions. Albuhaisi
85   et al. (2023) used 12 flux stations available between 2015 and 2018 from the FLUXNET-CH4 database to calibrate the scaling parameter of their boreal emission models, but the two other parameters (Q_{10} and T_0) were set according to literature values.

In addition to this improvement in available methane flux data, new dynamic estimates of wetland area have emerged since the studies of Gedney (2004) and Bloom et al. (2017). These estimates are based on either satellite observations or hydrological models. The Wetland Area and Dynamics for Methane Modeling product (WAD2M), published by Zhang et al. (2021a), provides a complete dynamic map of wetlands, including peatlands. It is partly based on satellite data and is widely used in the community, especially for the GMB (Saunois et al., 2020). Xi et al. (2022) produced an ensemble of 28 wetland extent products derived from TOPMODEL, a hydrological model.

Recently, McNicol et al. (2023) developed a random forest framework (UpcH4) to predict CH_4 fluxes based on 43 wetland sites from the FLUXNET-CH4 database. This approach combined with WAD2M wetland surfaces estimates allowed them to provide independent global data-driven empirical upscaling of wetland CH_4 emissions.

Our study aims to revise the simplified process-based modelling approach for wetland methane emissions proposed by Gedney (2004), taking advantage of recent developments. The objective is to develop a model framework capable of assessing the main features of wetland methane emissions (annual budget, seasonal cycle, spatial distribution) on a global scale with a resolution of 0.25°x0.25°, with a focus on methane fluxes inter-annual variability. The Satellite-based Wetland CH_4 model (SatWetCH4) is based on a data-driven approach, mostly fed with satellite-derived datasets, to allow fast and easy sensitivity calculations. SatWetCH4 provides an independent estimate, and uses in situ eddy covariance data for model calibration. Particular attention has been paid to the proxy for available carbon. As methanogenic activity has been shown to be related to plant productivity (Bridgham et al., 2013), here we use a MODIS plant photosynthesis product to derive a $C_{substrate}$ dataset to assess the organic matter available for methanogenesis, as described in Sect. 2.1. The aim of deriving the $C_{substrate}$ product is to obtain a carbon product that 1) best represents the carbon available for methanogenesis, 2) is dynamic, 3) is based on satellite data, and 4) is independent of LSMs.

Section 2 presents the materials and methods, including the model, the satellite-based input datasets and the calibration procedure. Optimization results are presented in Sect. 3.1, followed by a site-level evaluation of the model in Sect. 3.2. The global-scale results for the period 2003-2020 are presented in Sect. 3.3. Section 4 examines the model's limitations and prospects for improvement given the current state of modeling.

2 Materials and Methods

2.1 Model description

We estimate the methane flux using the following formulation, similar to that of Gedney (2004):

$$F_{CH_4} = k f_w C_{substrate} Q_{10}(T)^{(T-T_0)/10} \tag{1}$$

where k is a scaling factor, f_w the wetland fraction of the pixel, $C_{substrate}$ the carbon content that is available for methanogenesis, and T the soil temperature. $Q_{10}(T)$ depends on Q_{10}^0 the temperature sensitivity of methanogenesis and T. It is defined by $Q_{10}(T) = Q_{10}^0{}^{T^0/T}$. T^0 is set to ~~273.15° K~~ 273.15 K, resulting in low emissions for frozen or near frozen soils. Consequently, Q_{10}^0 and k are the two parameters to be calibrated.

The substrate available in the soil for methanogenesis, $C_{substrate}$, is calculated independently, upstream of the model. It is constructed as a litter pool model scheme and depends on temperature, Net Primary Productivity (NPP) and varies with time. This $C_{substrate}$ is computed using the following equation :

$$\frac{dC_{substrate}}{dt} = NPP - K(T)C_{substrate} \tag{2}$$

In this scheme, the available substrate is assumed to originate mainly from photosynthesis, which is approximated as NPP. The second term represents the carbon loss due to soil heterotrophic respiration, which depends on a turnover rate function $K(T) = K^{ref}Q_{10K}^{(T-T_K^{ref})/10}$. K^{ref} reflects the reference turnover time, Q_{10K} the temperature sensitivity coefficient of respiration, and T_K^{ref} the reference temperature. Incubation experiments (Parton et al., 1987; Khvorostyanov et al., 2008; Schädel et al., 2014) provided estimates of K between 0.2 and 2.5 yr^{-1}, corresponding to a residence time of carbon in soils between 0.4 and 5.5 years. Therefore, to obtain a consistent K, the model parameters are set to $K^{ref} = 1/2yr = 0.5yr^{-1}$, $T_K^{ref} = 303.15°K$$T_K^{ref} = 303.15\ K$, and $Q_{10K} = 2$.

The global estimate of $C_{substrate}$ is established in advance by discretizing Eq.2 at monthly time steps. The $C_{substrate}$ was primarily run for 100 years to reach an equilibrium stage, constrained with 2001 NPP values obtained from remote sensing data (Zhang et al., 2017) detailed in Sect. 2.3. NPP data between 2003 and 2020 were then used to estimate $C_{substrate}$ over the same period on a monthly scale.

2.2 In situ data

Figure 1. Sites distribution per **a.** length of available observation period, **b.** wetland type and **c.** geographic location. In map **c.**, because of their close location (few km) some sites overlaps. Site color depends **a.** and **b.** on site latitude : boreal (55°N-90°N), temperate (30-55°N or °S), or tropical (30°S-30°N), and **c.** on wetland type.

135   Eddy covariance time series of methane fluxes from different databases were combined in order to use robust, continuous and the longest methane flux monitoring period recorded at each site. In situ data from 58 wetland sites were collected from FLUXNET-CH4 (Delwiche et al., 2021), AmeriFlux (Baldocchi et al., 2001), EuroFlux (Valentini, 2003). In addition, data for BW-Gum and BW-Npw sites were obtained from the UK Centre for Ecology & Hydrology website, and IN-Pic data were provided through personal exchanges with the principal investigator, P. Gnanamoorthy. Some ancillary variables of interest for

140   methane emission modelling (e.g. soil temperatures, WTD, SWC, precipitation) are available at some of the sites. Links to the sources used are given in Supplementary Table S1 and the full list of sites and details are listed in Supplementary Table S2.

    The length of the time series, wetland types, and location of the sites are presented in Fig. 1. Despite the construction of the most comprehensive database from recent literature, the global distribution of methane eddy covariance tower sites shows significant heterogeneity. The majority of sites, 46, are located at latitudes greater than 30°N, with 36 sites in North America

145 and 10 sites in Europe. Only 11 sites (19%) are located in the tropical band 30°S-30°N, including, for example, only 2 sites on the entire African continent, which are only a few kilometers apart, and 2 sites in South America. In addition, Fig. 1.a highlights the heterogeneity in measurement duration, with tropical sites having a median measurement duration of 1.6 years, as contrasted with 2.7 and 3.2 years for boreal and temperate sites, respectively. It is also important to note that sites can be very close to each other (within a few kilometers). This uneven distribution of sites introduces a bias in the global calibration

150 of the model. In particular, tropical wetlands are severely underrepresented, although they are expected to account for about ~75% of global wetland methane emissions (Saunois et al., 2020).

To ensure a homogeneous dataset, the same data processing was applied to the raw data. The 30 min raw data points were extracted, and the variable units were unified. Outliers are removed for all variables, including ancillary data, notably for methane fluxes, for each site and day, data outside of $\overline{F_{CH4day}} \pm 5std_{F_{CH_4}day}$ are excluded. Finally, daily averages are

155 calculated for all variables, and monthly averages are only calculated if more than 4 days of data are available in a given month. A monthly time scale was chosen for this study because it effectively captures seasonal variations while minimizing the influence of variables that operate at shorter time intervals, such as daily or multi-day changes in atmospheric pressure, or diurnal cycles in vegetation and temperature (Knox et al., 2021). Furthermore, as our model is a one-step model without differentiation between production and emissions, the monthly time scale also mitigates potential errors due to time lags

160 between methane production and transport (Ueyama et al., 2023).

This results in a dataset of 2354 monthly mean methane fluxes associated to their available ancillary data.

2.3 Global forcing datasets

2.3.1 MODIS PSnet data

To derive $C_{substrate}$ estimates, as defined in Eq.2 in Sect. 2.1, we use PsnNet from the MODIS MOD17A2HGF v6.1 dataset

165 (Running and Zhao, 2021). The PsnNet dataset represents NPP, except that it excludes growth and maintenance respiration costs. This product is based on satellite Fraction of Photosynthetically Active Radiation (FPAR) data, a reanalysis meteorological dataset, and land cover classification.

The data cover the period from 2000 to the current year, but data for 2002 are not available, so only the period from 2003 to 2020 has been used in this study. The PsnNet product has been regridded from the native 500 m resolution to a 0.05° product

170 used for model optimization at the site level, and to a 0.25° resolution product used for the global simulation. In terms of timescale, monthly averages were estimated from the initial 8-day product.

2.3.2 ~~ERA5~~ ERA5-Land soil temperature

For the soil temperature variable, monthly averaged data from ERA5-Land (Muñoz-Sabater et al., 2021), available at ~~https://cds.climate.cop~~ //cds.climate.copernicus.eu/, are used. The temperature in the 7-28 cm soil layer is selected, denoted as *lay2*. These data are

175 available from 1950 to the present with a resolution of 0.1°x0.1°. A comparison of in situ soil temperature measurements with ~~ERA5 land~~ monthly ERA5-Land *lay2* closest 0.1° pixel is detailed in the Supplementary Fig.~~S1~~S2, showing good agreement

between in situ and ~~ERA5~~ ERA5-Land soil temperatures, with in particular a high temporal correlation (r>0.9) and low RMSD (<2° K) for 37 of the 42 sites equipped with temperature probes.

2.3.3 Global wetland extent datasets

Two wetland areas are used to estimate global methane emissions. The Wetland Area and Dynamics for Methane Modeling (WAD2M) version 2.0 (Zhang et al., 2021a) describes the fraction of wetlands per pixel globally at a resolution of 0.25°x0.25° for the period 2000-2018 with a monthly time step. The dynamics of WAD2M are driven by the Surface Water Microwave Products Series (SWAMPS) (Jensen and Mcdonald, 2019), which relies on passive and active microwave satellite observations. Several static datasets are used to add non-inundated wetlands, such as peatlands, and to remove lakes, irrigated rice paddies (Zhang et al., 2021b). The second wetland map used is based on the TOPography-based hydrological MODEL (TOPMODEL). Xi et al. (2022) built an ensemble of 28 maps describing globally the fraction of wetlands per pixel at a resolution of 0.25°x0.25° for the period 1980-2020 at a monthly time step (Xi et al., 2021). A combination of 7 different soil moisture reanalysis datasets and 4 different surface wetland extent products were used to calibrate the model. Among the 28 products, we select here the version calibrated with ~~ERA5~~ ERA5-Land soil moisture data and the GIEMS-2 (Prigent et al., 2020) long-term maximum, as it shows the highest correlations of wetland area with the original wetland product (Xi et al., 2022).

2.4 Calibration method

The in situ methane fluxes at the sites were used to calibrate the SatWetCH4 model parameters k and Q_{10}^0. Model calibration at site level implies that each site is considered to be completely covered by wetland, resulting in a wetland fraction of 1 ($f_w = 1$). The flux equation to be optimized at site level is then $F_{CH_4} = kC_{substrate}Q_{10}(T)^{(T-T_0)/10}$. The $C_{substrate}$ product (described in Sect. 2.1) and ~~ERA5~~ ERA5-Land soil temperature (described in Sect. 2.3) are used as input variables by selecting the nearest pixels to the sites, at 0.05° for $C_{substrate}$ and 0.1° for ~~ERA5~~ ERA5-Land soil temperature respectively.

Least squares regression is performed simultaneously on all sites using the Broyden-Fletcher-Goldfarb-Shanno algorithm (Byrd et al., 1995). For sites with less than 12 months of data, a weight proportional to the number of monthly measurements is assigned to the site data. Sites with more than 12 months of data are given equal weights. The minimized cost function is :

$$J = \sum_{sites} w_{site} MSD_{site} = \sum_{sites} w_{site} \overline{(F_{CH_4obs} - F_{CH_4sim})^2_{site}} \tag{3}$$

where w_{site} is the site weight, MSD is the Mean Square Deviation, F_{CH_4obs} is the in situ methane flux observed at the sites, and F_{CH_4sim} is the methane fluxes simulated by the model. If the number of monthly methane flux measurements at the site, n_{site}, is greater than or equal to 12, $w_{site} = 1$ otherwise $w_{site} = \frac{n_{site}}{12}$. Different initial parameter sets for $k_{firstguess}$ (0.01, 0.1, 1, and 10) and $Q_{10firstguess}^0$ (1.5, 2.5, 3, and 4) are tested to evaluate the influence of the calibration initialization and to ensure the global nature of the found minimum.

3 Results

3.1 Optimized model parameters
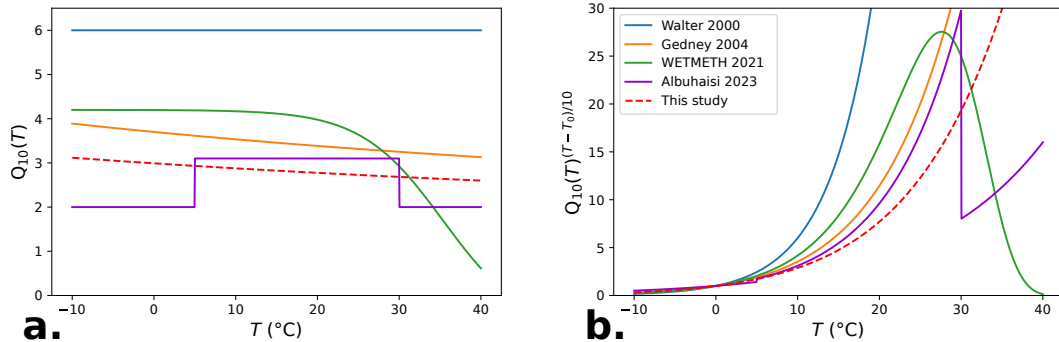
Figure 2. a. Comparison of $Q_{10}(T)$ formulation with Walter and Heimann (2000), Gedney (2004), WETMETH Nzotungicimpaye et al. (2021), and Albuhaisi et al. (2023). **b.** Effect of the different $Q_{10}(T)$ formulations when incorporated in the temperature dependency function.

The calibration is performed according to the method described in Sect. 2.4. The minimum cost function is found for $Q_{10,opt}^0 = 2.99$ and $k_{opt} = 3.097 \, 10^{-2} \, \mu g CH4/m^2/s$. The value of k_{opt} has no numerical meaning, as it is highly dependent on the units and order of magnitude of the substrate proxy we use. The $Q_{10}(T)$ formulation obtained from this calibration is compared with the literature values in Fig. 2a. Figure 2.b shows the influence of $Q_{10}(T)$ expressions when inserted in the temperature formulation $Q_{10}(T)^{(T-T_0)/10}$.

Walter and Heimann (2000) used a Q_{10} value of 6, based on the observations range available at the time. Nzotungicimpaye et al. (2021) in WETMETH proposed a $Q_{10}(T)$ formulation such that, when incorporated into the equation $Q_{10}(T)^{(T-T_0)/10}$, it indicates an optimal temperature range for methanogenesis around 25-30°C. Although we attempted a similar approach to formulate $Q_{10}(T)$, it resulted in minimal changes in the flux outcomes while increasing the complexity of the formulation and hindering the convergence of the cost function. Albuhaisi et al. (2023) used a fixed $Q_{10} = 3$, with a reduced value to $Q_{10} = 2$ for temperatures above 5°C or above 30°C to account for an optimal range. However, this results in abrupt transitions at these temperature thresholds (Fig. 2.b). This implementation may not be appropriate for global analysis, as tropical wetlands experience temperatures above 30°C, and such sudden changes do not reflect of physical reality.

Therefore, the Gedney (2004) formulation $Q_{10}(T) = Q_{10,opt}^0{}^{T_0/T}$ was used in SatWetCH4, resulting in $Q_{10}(T)$ from 3.12 (-10°C) to 2.60 (40°C), which is slightly lower than the Gedney (2004) value (3.89 at -10°C to 3.13 at 40°C). Our $Q_{10}(T)$ value contrasts with that of Walter and Heimann (2000) ($Q_{10} = 6.0$, no temperature dependence), but closely matches with the value chosen by Albuhaisi et al. (2023) for the 5°C-30°C range ($Q_{10} = 3.1$ for T between 5°C and 30°C, $Q_{10} = 2.0$ below 5°C or above 30°C). Consequently, similar $Q_{10}(T)^{(T-T_0)/10}$ curves are observed in Fig. 2.b between our estimate and those of Gedney (2004), and the 5-30°C range of Albuhaisi et al. (2023), although our formulation exhibits slightly lower values.

This would result in a slightly lower increase in methane fluxes with soil temperature. The $Q_{10}(T)$ found in this study is also in agreement with meta-analysis of Q_{10} defined from in situ data, e.g., 2.8 in Kuhn et al. (2021) and 2.57 in Delwiche et al. (2021).

230 **3.2 Evaluation of the model performance at site scale**
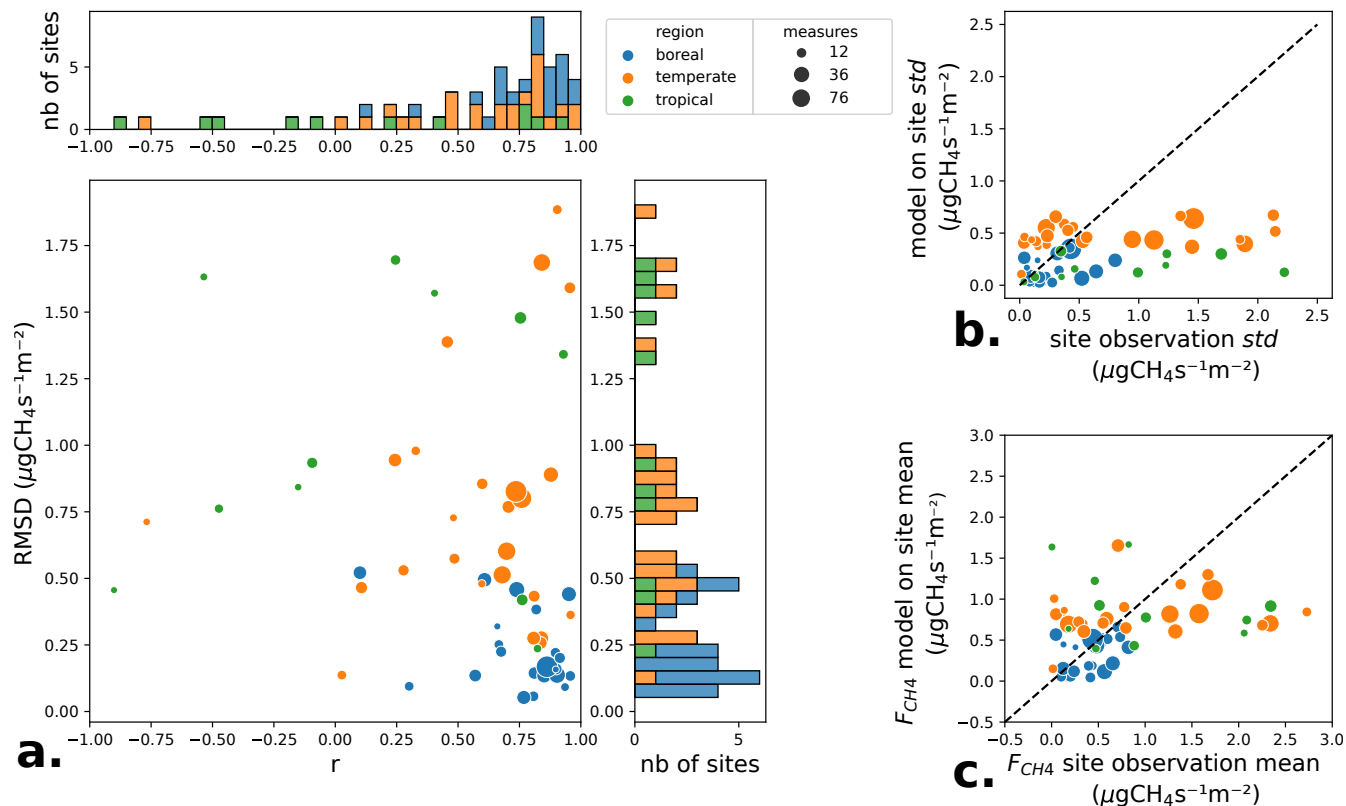
Figure 3. Comparison of methane fluxes modeled at site level with observations. Each site is represented by a point, its location by its color, while site number of measurements are represented by point sizes. **a.** Temporal correlation (r) and RMSD between model and observation. **b.** Standard deviation (std) of model fluxes in function of standard deviation of observation. **c.** Mean of model fluxes in function of mean of observation.

To evaluate the SatWetCH4 model, we run it at the site scale with the optimized parameters, setting $f_w = 1$ in Eq.1, and using the variables values from the pixels closest to the site, i.e. at 0.05° for $C_{substrate}$ and at 0.1° resolution for ~~ERA 5 temperature~~ ERA5-Land temperature (resulting monthly estimates can be found in Supplementary Fig. S1). Note that the difference in spatial resolution between the site level, i.e. the footprint of the flux towers (up to 1km^2), and the resolution of the available

235 substrate (0.05°x0.05°~25km^2) limits the comparison. The temperature is more homogeneous and its aggregation at 0.1° is less

problematic. Figure 3 compares the in situ flux data with the modeled site-level output. Figure 3.a. shows the Root Mean Square Deviation (RMSD) and the temporal correlation (r) between the observations and the simulated flux. It indicates a generally lower average RMSD in the boreal zones (average RMSD of 0.23 μgCH4s^{-1}m^{-2}) compared to the temperate zones (average RMSD of 0.8 μgCH4s^{-1}m^{-2}) and the tropics (average RMSD of 1.1 μgCH4s^{-1}m^{-2}). It shows that the model captures the seasonality of emissions well for boreal sites (r > 0.7 for 16/22 boreal sites), less well for temperate sites (r > 0.7 for 11/25 sites) and poorly for tropical sites (r > 0.7 for 4/11 sites, with 5/11 sites having r < 0). Figure 3.b and Fig. 3.c display the amplitude variations (standard deviation) and mean values of the observed and modelled fluxes. The mean fluxes are consistent with the in situ values (Fig. 3.c), while the standard deviation (std), which represents the amplitude of the seasonal variation, is underestimated for fluxes with std greater than 1 μgCH4s^{-1}m^{-2} (Fig. 3.b).

Thus, the model reproduces boreal fluxes better than temperate and tropical fluxes. This results in higher RMSD values for tropical and temperate zones, as shown in Fig. 3.~~e~~a., although these higher RMSD values are also due to generally larger fluxes in the tropics. The underestimation of fluxes in the tropics is partly due to the sampling bias mentioned in Sect. 2.2: only a small proportion (19%) of the sites are located between 30°S and 30°N, and they have shorter monitoring periods, resulting in a cumulative weight of 18.5% in the cost function J (boreal sites weight 38% and temperate sites 43%). Furthermore, the mechanisms driving the temporal variations in tropical methane flux are certainly poorly represented in the model, as discussed in Sect. 4.

3.3 Methane emissions from wetlands on a global scale

After calibrating k_{opt} and $Q^0_{10,opt}$, we run the SatWetCH4 model (Eq.1) on a global scale for the period 2003-2020 at a resolution of 0.25°x0.25° with forcing datasets $C_{substrate}$, ~~ERA 5~~ ERA5-Land soil temperature and either WAD2M or TOP-MODEL product for wetland extent at the same resolution. In the following, we compare the wetland emissions derived from SatWetCH4 in terms of total global methane emissions, spatial distribution and temporal variations with Bloom et al. (2017), UpCH4 (McNicol et al., 2023), and the ensemble mean of the GMB (Saunois et al., 2020).

3.3.1 Comparison of the spatial distribution of the wetland extents
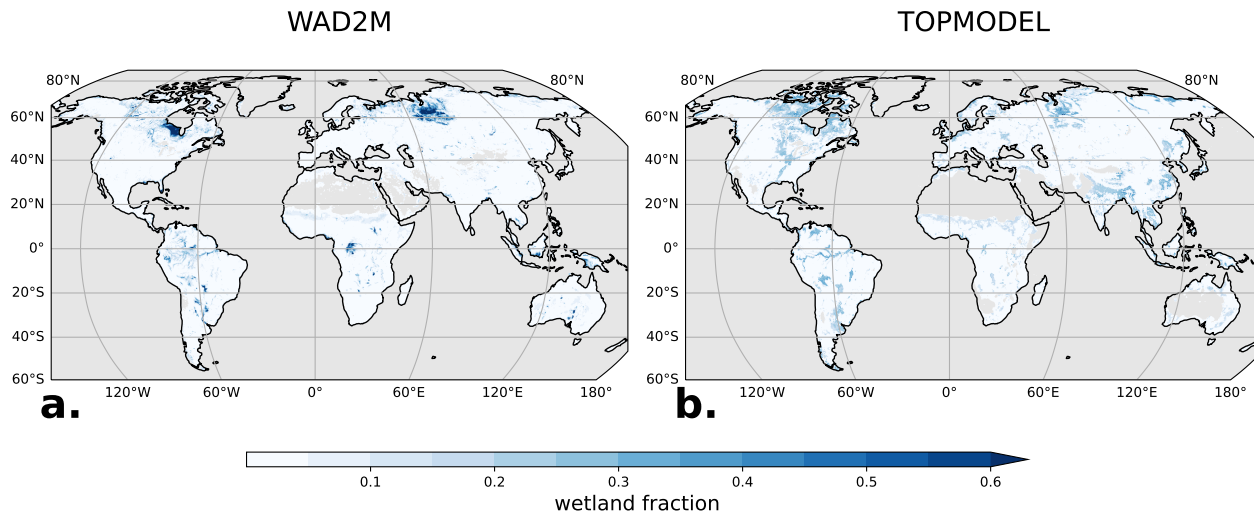
Figure 4. Wetland fraction 2003-2020 ~~mean~~ annual mean of **a.** WAD2M and **b.** the model TOPMODEL.

For both products, the monthly average of surface extent served to derive a Mean Annual Mean (MAmean) and Mean Annual
260   Maximum (MAmax) by selecting for each 0.25° pixel the mean or maximum of the typical 12-month seasonality. The maps of
MAmean of both wetland extent products are presented in Fig. 4. WAD2M has a global MAmean of 4.21 Mkm^2 and a MAmax
of 6.76 Mkm^2 over 2003-2020, while TOPMODEL is lower with 3.04 Mkm^2 and 5.12 Mkm^2 respectively.

This discrepancy in the value of the total area is mainly due to the methodology employed to construct the products. First,
WAD2M is known to overestimate coastal areas due to ocean contamination by nearby ocean pixels in the original SWAMPS
265   data (Pham-Duc et al., 2017; Bernard et al., 2024). Second, WAD2M includes non-inundated wetlands, such as peatlands,
whereas TOPMODEL represents only inundated wetlands. Indeed, Xu et al. (2018) estimate that peatlands cover around 4.23
Mkm^2. In fact, WAD2M wetland fraction over peatland areas (e.g. Hudson Bay, Congo, Siberian lowlands, Amazon floodplain)
is larger than in TOPMODEL (Fig. 4). Note that some boreal peatlands in WAD2M are masked by snow cover in winter, which
explains the lower MAmean than the global peatland extent. There are other large spatial differences between the two datasets.
270   Of concern in WAD2M is the substantial detection of water over Australia, a predominantly desert and semi-arid region,
and subequatorial Africa (Sahel). Wetlands and deserts have similar microwave signatures, explaining the possible confusion
(Pham-Duc et al., 2017). Finally, TOPMODEL shows higher scattered extents over North America, India, and China than
WAD2M.

3.3.2 $C_{substrate}$ ~~$C_{substrate}$~~ spatial distribution
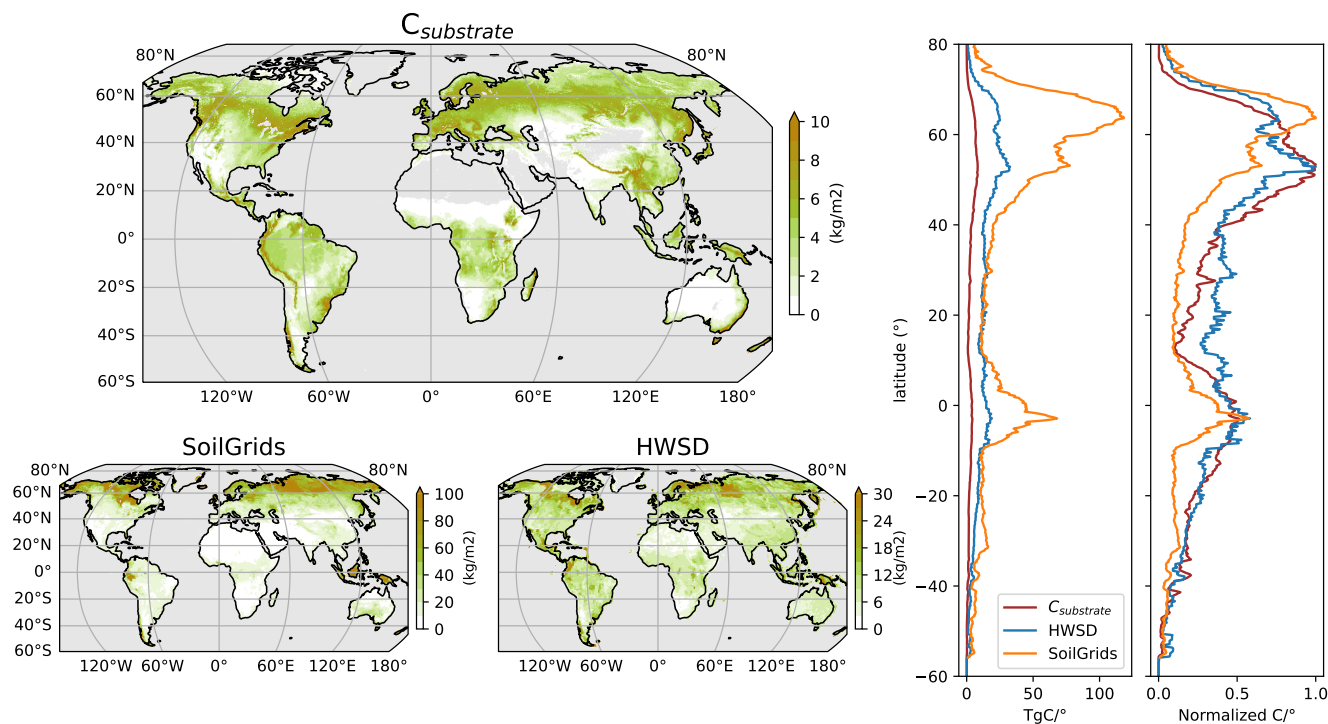
Figure 5. ~~2003-2020 mean of the derived~~ Derived $C_{substrate}$ product (top left) ~~and its latitudinal profile (middle) and the latitude profile normalized by~~ showing the ~~latitudinal maximum (right) along with~~ 2003-2020 mean, alongside two SOC databases (bottom left and middle) for the 0-100 ~~-~~cm layer: HWSD (Wieder, 2014) and Soilgrids (Hengl et al., 2017). The corresponding latitudinal and normalized latitudinal profiles are displayed (right panels). Normalization is achieved by dividing by the latitudinal maximum for each product.

275   The 2003-2020 mean map of the $C_{substrate}$ product is shown in Fig. 5. This product is used as a representation of the soil carbon substrate available for methanogenesis. It should be noted that there are no analogous products for evaluation. We suggest a comparison with global estimates of 0-100cm SOC stocks derived from the World Soil Database (HWSD) (Wieder, 2014) and SoilGrids (Hengl et al., 2017) to see differences between our proxy for available substrate compared to total organic carbon stocks. The latitudinal distribution and the latitudinal distribution normalized by the latitudinal maximum of the three

280   products are shown on the right side of the figure.

     The numerical values of $C_{substrate}$ tend to be consistently lower than those of the SOC estimates, differing by about an order of magnitude. This observation aligns with the fact that elevated SOC values, which are particularly common in peatlands, do not translate into a proportionally increased production of CO_2 or CH_4 emissions. In fact, the slow decomposition of organic matter in peatlands leads to carbon sequestration in soils over millennia (Clymo et al., 1998). It is important to emphasize that

285 the order of magnitude of the numerical value of $C_{substrate}$ is of limited significance, since the calibration of the k factor is used for the methane flux calculation. The critical focus is on the spatial variations and temporal dynamics of $C_{substrate}$ for accurate methane flux assessments.

The $C_{substrate}$ product shows a small seasonal variation (about 5% at global and basin scales), implying that its contribution is mainly of spatial nature. Indeed, we observe a different spatial distribution between the three products. SoilGrids and HSWD 290 tend to show more localized high carbon values in regions where peatlands are abundant, such as the western Siberian lowlands or the northern part of America, or for SoilGrids in Indonesia. $C_{substrate}$ presents a more homogeneous distribution, with moderate values in boreal and temperate regions. It consistently shows no or low available substrate values over bare soil regions (Sahara, Australia). In light of these considerations, $C_{substrate}$ appears to be a valuable candidate for estimating soil carbon availability.

 ### 3.3.3 Spatial variations of methane emissions
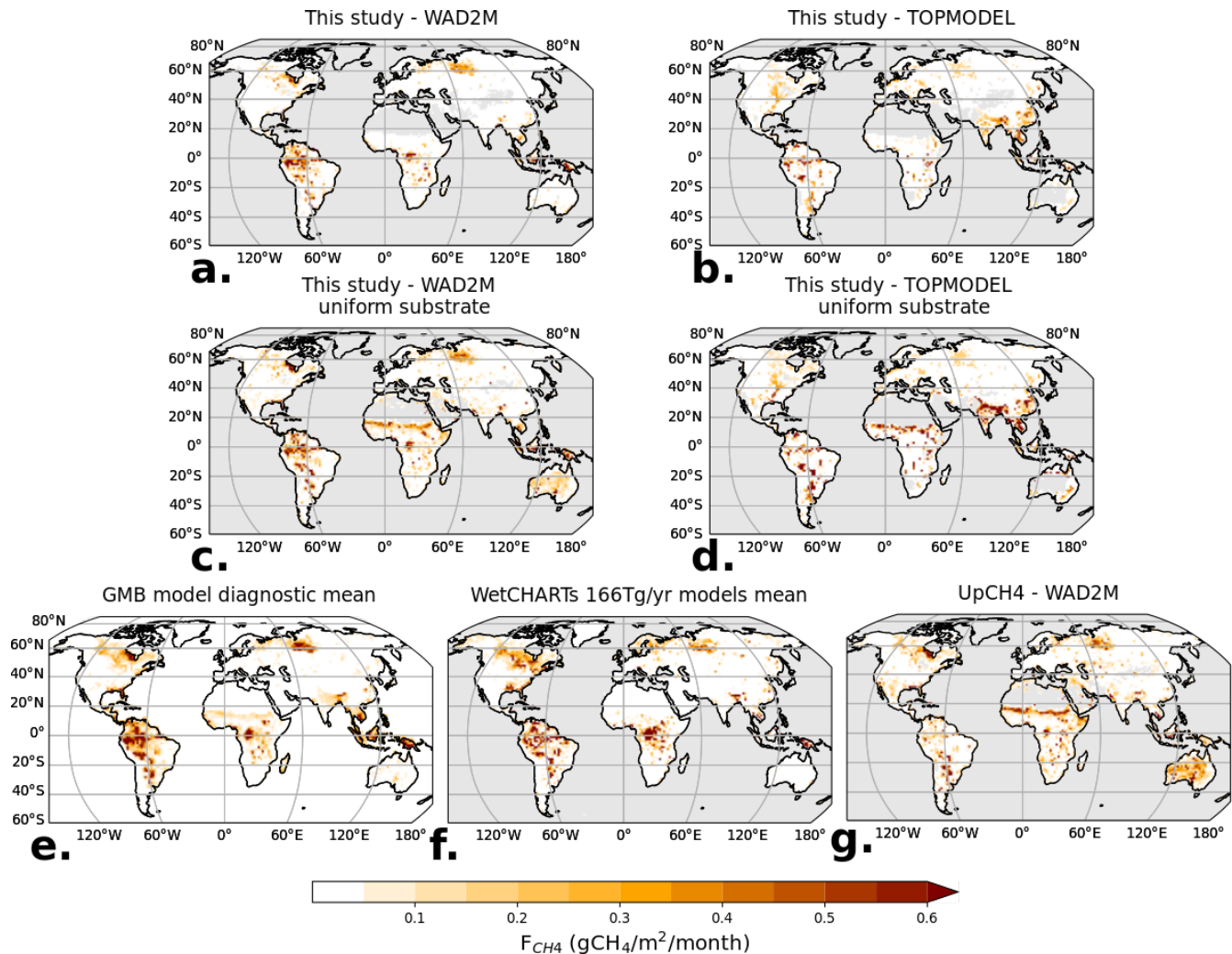
Figure 6. SatWetCH4 modeled mean methane ~~emission using~~ emissions: **a.** using WAD2M and **b.** TOPMODEL wetland surfaces~~.~~ ~~SatWetCH4 emissions obtained using~~ ; and with a uniform substrate ~~—~~ (i.e., $C_{substrate}$ = 1~~— and~~) **c.** using WAD2M ~~or~~ and **d.** using TOPMODEL. Emissions obtained by **e.** the mean of GMB diagnostic models, **f.** the mean of WetCHARTs ensemble, and **g.** UpCH4 upscaling.

The methane fluxes derived from SatWetCH4 are strongly influenced by the spatial patterns of the wetland extent used: the differences between WAD2M and TOPMODEL mentioned in Sect. 3.3.1 are partly reflected in the output fluxes (Fig. 6a. and b.). In fact, the parameter f_w is directly a multiplicative coefficient in the flux calculation in Eq.1. In particular, peatland

regions emit more in the WAD2M version, and the Ganges and Yangtze basins show much more intense methane emissions when TOPMODEL is used.

We assess the sensitivity of SatWetCH4 model to the $C_{substrate}$ product derived from the NPP (Eq.2) by comparing the results from SatWetCH4 reference run (with $C_{substrate}$) and a run that considers a uniform substrate ($C_{substrate}$=1 over the globe). Note that to do this, we had to calibrate the model parameters k and Q_{10}^0 using the same method described in Sect. 2.4. ~~The found~~, resulting in a lower $Q_{10,opt}^0$ ~~is lower~~ (1.83 instead of 2.99). ~~Figure 6.c and d show average emissions assuming a uniform substrate for methanogenesis, run with WAD2M or TOPMODEL.~~ The spatial distribution is then very different (Fig. 6.c and d), depending only on the wetland extent dataset and weighted by temperature. In particular, emissions are significantly higher in subequatorial Africa (Sahel) with both wetland datasets when no substrate product is included in the model. In fact, $C_{substrate}$ is small over this region due to a small value of the MODIS PsnNet input (Fig. 5). Over Australia we observe significantly higher fluxes with WAD2M when $C_{substrate}$ is not considered. This shows an overestimation of WAD2M wetland detection in the Australian desert, which is mitigated by the small $C_{substrate}$ over this region when $C_{substrate}$ is considered instead of the uniform substrate (Fig. 5).

The ensemble mean of the GMB LSMs simulations (Saunois et al., 2020) is shown in Fig. 6.e. Detailed maps of the individual model outputs are provided in the Supplementary Fig. ~~S3~~S4, together with the LSMs output standard deviation map. Comparison is made with GMB LSMs run in diagnostic mode, i.e. all LSMs were run with the same wetland area WAD2M standardized to the same 1°x1° grid for consistency. In addition, Fig. 6.f shows the model mean of the WetCHARTs ensemble (Bloom et al., 2017), which considers different wetland extent products, but not WAD2M. In the WetCHARTs ensemble, three scaling factors are tested to amount to a global mean annual flux of 124.5, 166 or 207.5 TgCH4 yr^{-1} (Saunois et al. (2016) lower, mean and upper estimates). Here we have selected only those members of the ensemble that were calibrated to the mean budget (166 TgCH4 yr^{-1}). The standard deviation map of methane emissions from the WetCHARTs ensemble is also included in Supplementary Fig. ~~S3~~S4. Figure 6.g shows the flux estimates of UpCH4 (McNicol et al., 2023). The UpCH4 estimate is defined using WAD2M wetland extent and is independent of the GMB LSMs.

The spatial distribution of the SatWetCH4 emissions run with WAD2M is similar to the average of the LSMs ensemble run with the same wetland extent over America, Australia, and Europe. However, there is considerable variability in the spatial emissions between models in some regions, including the Siberian lowlands (Ob), Australia, India, and over sub-equatorial Africa, even though the same water surface map is prescribed.

In subequatorial Africa (Sahel), emissions are highly uncertain between models. The different diagnostic outputs of the GMB LSMs (run with WAD2M) show a wide range of emissions (Supplementary Fig. ~~S3~~S4). Four of the diagnostic LSMs have low emissions (<0.1 gCH4/m^2/month), while the other nine have moderate to high emissions (0.1 to 0.5 gCH4/m^2/month). Like the first group of diagnostic LSMs, the ensemble mean of WetCHARTs (which is based on a different wetland extent than WAD2M) and the SatWetCH4 model predict almost negligible emissions (<0.05 gCH4/m^2/month). The GMB LSMs are also run in prognostic mode (Saunois et al., 2020), i.e., using their own calculation of wetland extent (not shown here). Prognostic results from 10 out of the 11 GMB LSMs show insignificant emissions over Sahel (<0.05 gCH4/m^2/month). The UpCH4 estimates, which are established with WAD2M, predict very high fluxes over the Sahel (>0.5 gCH4/m^2/month). Therefore, it

appears that this emission overestimation in the Sahel region might be due to the wetland extent, WAD2M, that is employed

335 for the GMB model intercomparison study and UpCH4. This wetland detection in the Sahel is due to desert contamination in this region (see Sect. 3.3.1) In SatWetCH4, there is a compensation between the high wetland fraction, f_w, defined using WAD2M, and the low $C_{substrate}$ value for the Sahel area. As the PsnNet parameter of the MODIS parameter is low in this zone, the $C_{substrate}$ dataset estimates a very low available carbon. The number of measurements available to evaluate the different methane emission simulations in the Sahel region, and in general over the tropics, is limited (difficult to access areas,

340 no flux towers, no in situ flux or concentration measurements).

In Australia, desert areas are also mistaken to inundated area in WAD2M. Most diagnostic LSMs outputs show Australia with low emissions. However, some models produce surprising spatial patterns in Australia, especially in desert regions for LPJ-GUESS and TEM-MDM. UpCH4 also presents high fluxes in most of the country. However, other models, including ours, certainly mitigate this issue by reducing emissions due to other parameters such as vegetation cover or hydrological settings,

345 thereby compensating for the problem of misclassification of wetlands.

Northern India also exhibits lower emissions in SatWetCH4 when run with WAD2M compared to the GMB average. Supplementary Fig.S3 S4 indicates that this elevated average is mainly due to one model, DLEM, with very high emissions in this region, while the other models show emissions similar to ours. This discrepancy raises questions about the representation of rice paddies in the DLEM model, despite the forcing of water surface dynamics.

350 Overall, the spatial distribution of SatWetCH4 run with WAD2M globally aligns with the ensemble of LSMs, WetCHARTS, UpCH4 and their uncertainties. We have discussed that when SatWetCH4 is run with TOPMODEL, different spatial patterns emerge, which are no less surprising when compared to the variations observed within the GMB LSMs ensemble, WetCHARTs ensemble, and UpCH4 simulations.

3.3.4 Total methane emissions, latitudinal and seasonal variation of methane emissions
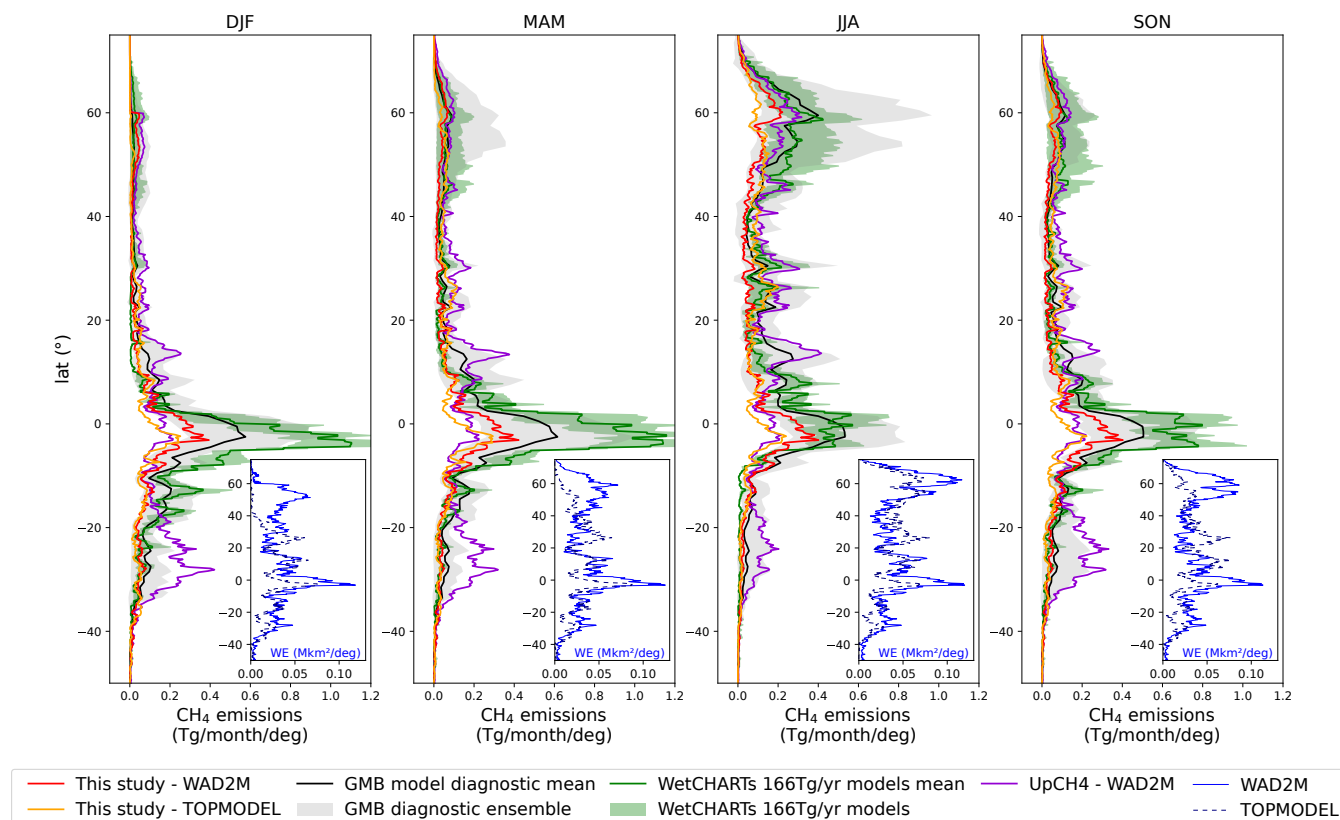
Figure 7. Latitudinal distribution depending on the season of wetland methane emissions from SatWetCH4 run with WAD2M (red) or TOPMODEL (orange), from LSMs (filled grey) with LSMs average (black), from WetCHARTS models calibrated with $166\,\mathrm{Tg\,CH_4/yr}$ budget (filled green) with ensemble average (green), and from UpCH4 (violet). WAD2M and TOPMODEL wetland extents seasonal mean are also presented in bottom-right box inserts (blue resp. solid and dashed lines). LSMs estimates are those contributing to the GMB (Saunois et al., 2020), all run with the same wetland extent product (WAD2M). All representations are 2003–2020 seasonal means.
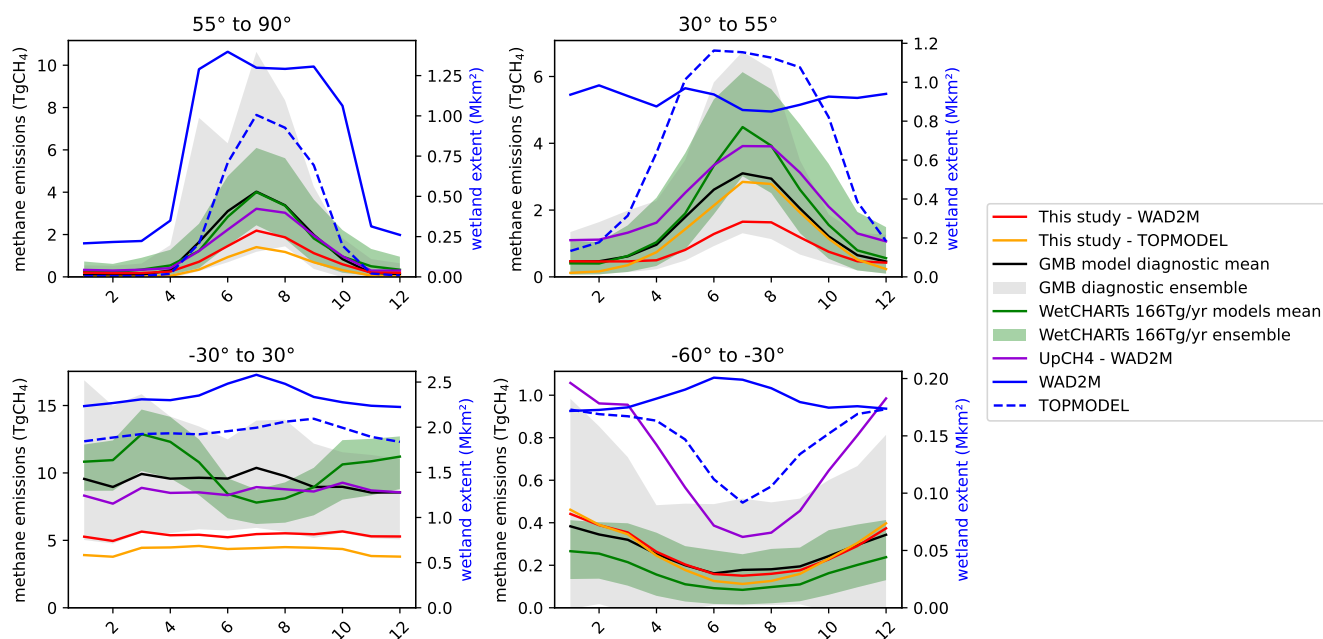
Figure 8. 2003-2020 CH$_4$ emission mean per month per latitudinal band from SatWetCH4 run with WAD2M (red) or TOPMODEL (orange), from LSMs (filled grey) with LSMs average (black), from WetCHARTS models calibrated with 166 Tg CH$_4$/yr budget (filled green) with ensemble average (green), and from UpCH4 (violet). WAD2M and TOPMODEL monthly wetland extent 2003-2020 means are presented in blue. LSMs estimates are those contributing to the GMB (Saunois et al., 2020), all run with the same wetland extent product (WAD2M).

355 Figure 7 shows the latitudinal distribution per season for SatWetCH4 run with WAD2M and TOPMODEL, as well as the GMB LSMs, WetCHARTs ensemble, and UpCH4 estimates. The monthly variation for emissions estimates and wetland extent per latitudinal band is shown in Fig. 8. Note that the WetCHARTs models are calibrated to the GMB annual budget and are therefore not independent in terms of methane emission amplitude. SatWetCH4 is in the lower range of the GMB LSMs (grey areas), or even slightly below this range in the 30°S-30°N band. The total annual budget of SatWetCH4 wetland emission estimate

360 averages 85.6 Tg CH$_4$ yr^{-1} with WAD2M (resp. 70.3 with TOPMODEL), which is lower than the range of the GMB LSMs estimates (102 to ~~181~~ 182 Tg CH$_4$ yr^{-1}) and the UpCH4 estimates (146 Tg CH$_4$ yr^{-1}) even if the same wetland extent is used. This discrepancy can be explained by 1. an underestimation of methane fluxes by SatWetCH4 especially of tropical fluxes (discussed in Sect. 3.2 and in the following paragraph) and 2. the consideration by WAD2M of desert regions as inundated areas, leading to methane fluxes overestimation in Australia and Sahel in UpCH4 and some diagnostic LSMs (see discussion

365 Sect. 3.3.3, Fig. 6, ~~S3~~ S4 and 7). Indeed, Sahel and Australia represent 33.4 out of the 146 Tg CH$_4$ yr^{-1} estimated by UpCH4 using WAD2M, while these regions represent 4.5 Tg CH$_4$ yr^{-1} in SatWetCH4 using WAD2M.

The scarcity of site-level data in tropical regions, coupled with the absence of tropical peatlands and floodplain sites, has undoubtedly contributed to the uncertainty associated with the calibration of parameters. Furthermore, the use of site-level

calibration for tropical wetland emission may result in an underestimation at the regional or global scale. This is due to the fact
that dynamic wetland mapping products account for saturated or inundated areas, whereas site-level measurements conducted
during the dry season are likely to underrepresent the emission intensity of saturated areas. Consequently, the parameters
calibrated from dry season measurements may underestimate emission intensity when multiplied by the area of saturated
wetlands. This is a less significant issue in temperate and Arctic regions, where the wet seasons occur in summer and there is
minimal emission in winter. As the number of tropical sites increases, future studies could consider refining the calibration for
the tropics, for example, by only using wet season measurements for calibration.

Note that this difference in total emissions could be easily resolved by calibrating the k parameter to the total emissions of
the mean GMB LSMs if we need to constrain total emissions, as it has been done previously by Bloom et al. (2017); Gedney
et al. (2019).

SatWetCH4 simulation with TOPMODEL estimates lower emissions in the tropical and boreal bands compared to the simulation with WAD2M (Fig. 7). This is consistent with the smallest wetland extent of TOPMODEL over these regions, as
non-inundated peatlands are not considered in TOPMODEL. Note also the higher fluxes obtained in the simulation with TOPMODEL than with WAD2M around 25-30°N, due to the larger wetland extent of TOPMODEL over Asia. The latitudinal distribution of SatWetCH4 (Fig. 7) is consistent with the distribution of the LSMs ensemble, except for the ~~African subequatorial~~ Sahel band mentioned earlier. SatWetCH4 reproduces similar seasonal changes as the GMB LSMs (Fig. 7), while the latitudinal
distribution of the WetCHARTs ensemble presents larger emissions in the 10°S-5°N band in the DJF, MAM and SON seasons
(mainly due to high emissions in the Congo region, visible in Fig. 6). UpCH4 presents a different latitudinal distribution, with
higher fluxes in the 15°N and 35°S-15°S bands. These are respectively due to the Sahel and Australia artifacts mentioned
above. UpCH4 has lower fluxes in the tropical 10°S-5°N band (due to the Amazon and the Congo basins).

This different seasonal cycle in the tropical band (30°S-30°N) for ~~WetWHARTs~~ WetCHARTs ensemble is also visible on
Fig. 8, while there is an absence of a pronounced seasonal pattern, both in terms of emissions and in terms of wetland extent
for our model and the GMB models. This difference in tropical seasonal cycle could be due to the wetland extent used in
WetCHARTs. For the boreal region (55-90°N), we find that the seasonal variation of the simulated emissions from our model
is close to that of most GMB LSMs, as it is in the northern temperate band (30-55°N). However, the wetland extents of WAD2M
and TOPMODEL show very different seasonality, particularly in the northern temperate band (30-55°N), where WAD2M has
a more stable wetland extent than TOPMODEL. Indeed, the methane emission seasonality in the boreal and temperate regions
is mainly driven by temperature, which explains these similar seasonal cycles in emissions, although the seasonal cycles in
wetland extent are different. For the southern temperate band (60°S-30°S), WAD2M and TOPMODEL exhibit contrasting
seasonality in wetland extent, but the simulated seasonal variations in emissions are close because, as expected, temperature
drives the variability of methane fluxes in this temperate region.

 3.3.5 Inter-annual variability in methane emissions at basin scale
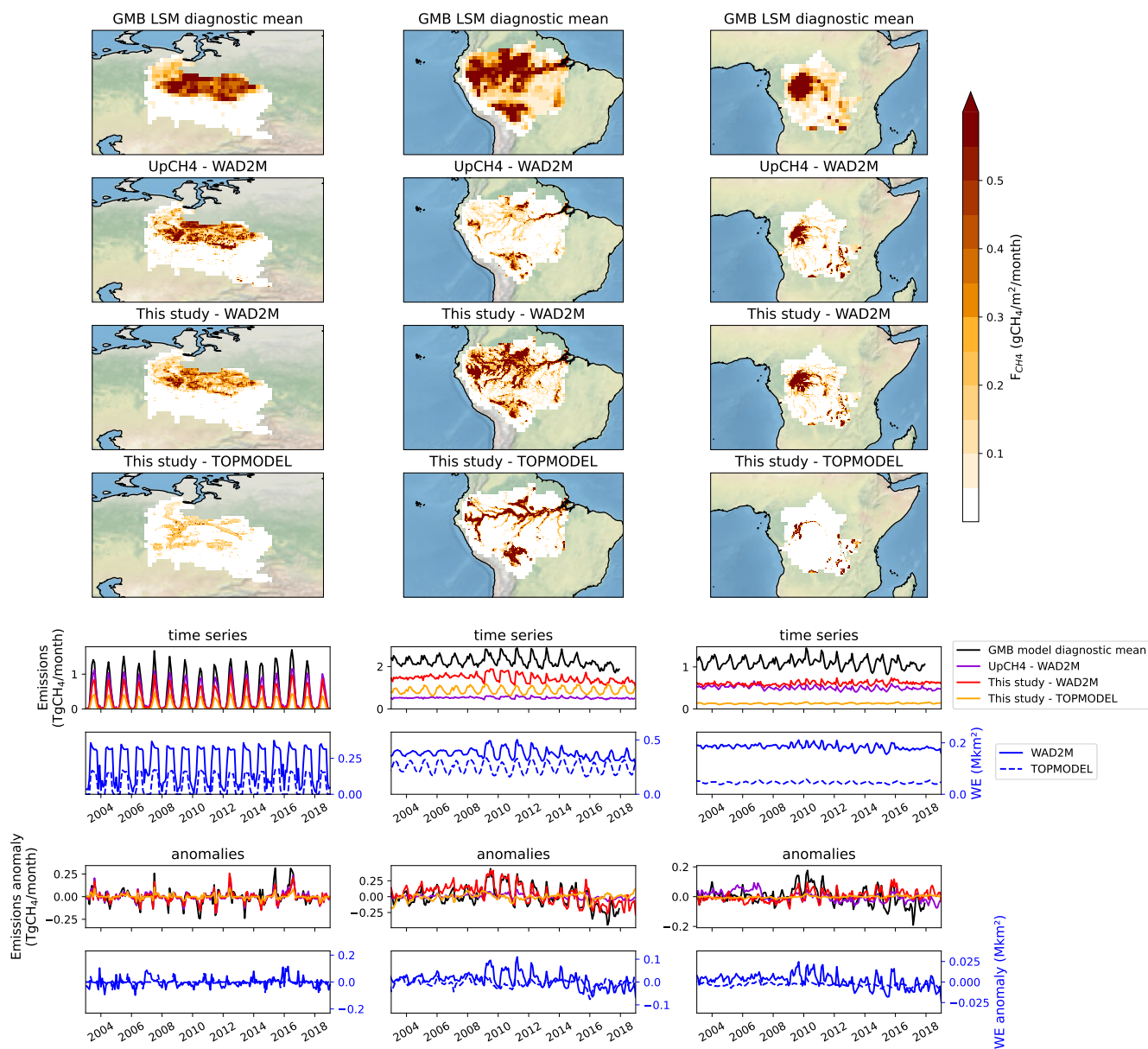
Figure 9. Methane emissions for different basins: the Ob, the Amazon, and the Congo. The maps show the spatial pattern of methane emissions from the GMB LSMs mean, UpCH4 run with WAD2M, and SatWetCH4 simulations with WAD2M or TOPMODEL. The lower panels represent the sum of methane emission time series and deseasonalized anomalies over the basins of SatWetCH4 simulations with WAD2M (red) or TOPMODEL (orange), LSMs diagnostic mean (black), and UpCH4 simulation with WAD2M (Violet). All LSMs were run with the same WAD2M wetland extent. WetCHARTs ensemble is excluded here because its methane emissions estimates are rescaled to the average values of the GMB LSMs estimates.

Figure 9 depicts SatWetCH4 model, GMB LSMs and UpCH4 emissions simulated with WAD2M and their anomalies for three basins: the Amazon, the Ob, and the Congo. Also shown are wetland areas and their anomalies over these basins.

In the Amazon and Congo basins, notable amplitude irregularities were observed when using WAD2M in SatWetCH4 or UpCH4. Two regime changes are observed in the WAD2M extent around 2009 and 2014, probably due to inter-calibration problems caused by satellite changes in the original SWAMPS surface water product. Surprisingly, the average of the LSMs is less affected, even though the LSMs are forced with the same water surface. However, on closer examination of individual LSMs (see Supplementary Fig. S4S5), we see that some LSMs are as affected as SatWetCH4 by these inconsistent water surface changes, while others are less affected. We deduce that these models, which are not affected by the WAD2M temporal changes, must have parameters that interfere with the consideration of the wetland surface. TOPMODEL suggests more consistent time series in terms of wetland extent (softer variations), which also allows for more realistic variations in terms of emissions.

4   Model limitations and outlook

The simplified approach used here as a one-step model allows for some quick and easy simulations, representing major first order phenomena affecting methane emissions from wetlands. While presenting a smaller annual budget, due to a possible underestimation of the magnitude of emissions, we found that this formulation presents realistic spatial and temporal variations when compared to other more complex and computationally intensive models. By scaling the k factor to a target estimate, the discrepancy in global emissions could be easily resolved.
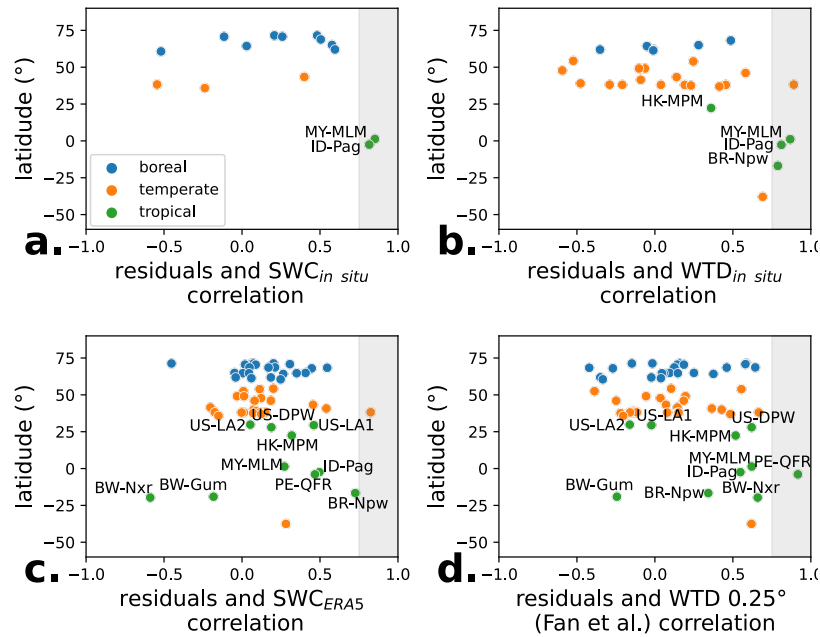
Figure 10. Correlation of residuals (observation-prediction) with **a.** in situ WTD, **b.** in situ SWC, **c.** 0.25° ~~ERA5~~ ERA5-Land SWC and **d.** 0.25° WTD (Fan et al., 2013). These residuals are calculated for a single site calibration of SatWetCH4 in order to remove the seasonal cycle that the model can capture through its variables (soil temperature and substrate availability). Grey background represents r>0.75.

Some refinements could be considered to improve the accuracy of the model. We found that the simulated temporal variability is less well captured at tropical sites than at temperate and boreal sites, as temperature does not drive seasonality in these regions. In fact, some studies (Kuhn et al., 2021; Knox et al., 2021) suggest that methane emissions in tropical regions are influenced by WTD. To investigate the flux dependence on a local water parameter, we calculated residuals from the single site calibration presented in Sect. 3.2. A residual is the difference between observed and predicted methane fluxes, and thus represents the error of the model at a given site at a given time. Figure 10 illustrates the correlation of different hydrological variables with the residuals. In the tropics, the missing variability appears to be strongly linked to soil water variations: 2 out of 2 (MY-MLM and ID-Pag) tropical sites monitoring SWC show a strong temporal correlation (r > 0.75) of residuals with locally measured SWC, and 3 out of 4 sites monitoring WTD (HK-MPM, MY-MLM, ID-Pag and BR-Npw) show a strong temporal correlation (r > 0.75) of residuals with locally measured WTD.

To test whether this site-level correlation could be used in SatWetCH4 model, we repeat this experiment using global datasets at 0.25° of SWC and WTD. For each site, we selected the nearest 0.25° pixel of the ERA5-Land monthly averaged SWC dataset (available at https://cds.climate.copernicus.eu/)), and the nearest pixel of the WTD from Fan et al. (2013) aggregated at 0.25° (as only one typical year is provided, this year is replicated for all years of the in situ flux measurement period). Figure 10.c and d. show the resulting correlation of these two variables at 0.25° with the residuals. None of the 11 tropical sites show an r > 0.75 between residuals and ~~ERA5~~ ERA5-Land SWC and only one site (PE-QR) shows an r > 0.75 between residuals and

0.25° WTD. This is due to the fact that these 0.25° datasets poorly represent the temporal variations measured in situ, as shown in Supplementary Fig. ~~S2 for the ERA5~~ S3 for the ERA5-Land SWC. SWC and WTD in wetlands have very spatially localized specificities and variations. Furthermore, the small number of sites available in the tropics (11) makes it even more difficult to find an empirical relationship with a water variable. We were unable to include this important parameter at SatWetCH4 model resolution of 0.25°. The 100m satellite-derived SWC obtained by Planet (De Jeu et al., 2014) could be examined and the model run at finer resolution. In fact, Albuhaisi et al. (2023) found an improvement in their model for the boreal region when using this high resolution product. Further research could be conducted to see if similar results are obtained in the tropics, where this parameter is most needed. Unfortunately, this product is not freely available.

It is worth noting that the site level comparison of modeled fluxes with observations assumes that the sites are all wetlands ($f_w = 1$), without any temporal variation. However, when the SatWetCH4 model is run, this wetland fraction is dynamic, introducing seasonality due to water and partially compensating for the lack of a local water parameter.

Another limitation is that the consistency of the time series of methane emission estimates at the catchment scale is strongly affected by errors in the WAD2M database. This makes it difficult to study inter-annual variability or trends. The TOPMODEL time evolution does not have these major temporal inconsistencies, but it is based on a hydrological model and not on satellite observations. It also does not include non-inundated peatlands. An improved satellite-derived dynamic wetland surface map would be crucial to address these issues while maintaining observational data in our data-driven approach.

The simplified SatWetCH4 model we have developed makes important approximations that imply important shortcuts. In particular, no distinction is made between methane production and emissions. This supposes that SatWetCH4 one-step equation includes production, oxidation, and transport in a single formulation, which are sometimes distinguished in some of the more complex LSMs (Wania et al., 2013; Morel et al., 2019; Salmon et al., 2022). Among the 3 pathways of methane transport in wetlands, including diffusion, ebullition and plant-mediated transport, plant-mediated transport is the dominant one (Ge et al., 2024). Ge et al. (2024) have recently published a comprehensive review of the role of plants in methane fluxes, showing their influence not only on methane transport but also on methane production and oxidation. Feron et al. (2024) also show that trends in methane flux changes at the site level depend on ecosystem and vegetation type. Accounting for the different vegetation classes therefore appears to be a possible improvement to our simplified approach.

A simple way to account for this in the SatWetCH4 model at a first order would be to fit the scaling factor k and/or Q_{10}^0 as a function of vegetation class or wetland type. Indeed, Q_{10} was found to depend on ecosystems (Chang et al., 2021). We performed such calibration tests, taking into account the wetland classification. However, the cost function either did not converge due to the small number of sites per category, or the result was highly dependent on few sites, thus overfitting results. In fact, eddy covariance flux towers measuring methane emissions are not evenly distributed around the globe and their distribution is highly skewed, as discussed in part 2.2. Some wetland categories are poorly represented, for example, there are only two mangrove sites. This scarcity of data makes this type of calibration highly uncertain. However, we can expect an improvement in the coming years, as in situ methane measurement is a rapidly growing field, as shown by the increasing number of flux towers along the years in the Supplementary Table S1. Future data, especially in the tropics, will be essential to better constrain the models and to include more processes into account. Some refinement of the Q_{10} function (here

$Q_{10}(T) = Q_{10}^0 T^{0/T}$ according to Gedney (2004)) could be envisioned, such as the incorporation of a hysteresis (Chang et al., 2021).

470   Despite the impossibility of analyzing temporal variation due to WAD2M issues, Fig. 9 informs us that the temporal variations of SatWetCH4 are more similar to GMB LSMs than UpCH4. This is consistent with the fact that SatWetCH4 is a - highly simplified - process-based equation, whereas UpCH4 relies on empirical flux upscaling using random forest. SatWetCH4 and UpCH4 approaches both provide new independent estimates of wetland emissions, while offering distinct perspectives. A deeper comparison of the fluxes modelled by SatWetCH4 and UpCH4 at the site level could serve understanding differences

475 between the simplification of complex processes represented by a fixed process equation (SatWetCH4) versus a pure machine learning data-driven approach (UpCH4). In addition, running both SatWetCH4 and UpCH4 with another wetland extent database would also serve to assess uncertainties and errors associated with WAD2M product and a better comparison of global methane emissions trends estimated by SatWetCH4 and UpCH4. Both methods are currently limited by the scarcity of eddy covariance flux data (McNicol et al., 2023), especially over important wetland methane emitting regions of the world, e.g., in

480 the tropics (Congo, Sudd, Amazon) and Russia (Siberian lowlands).

5   Conclusions

SatWetCH4 model was developed to simulate global wetland methane emissions at 0.25°x0.25° with a monthly time resolution. This data-driven approach was calibrated with 58 sites of eddy covariance flux data, allowing an approach independent of other estimates. Most of SatWetCH4 model input variables are derived from satellite observational products. In particular, a new

485 estimate of the substrate availability was derived using MODIS-derived NPP. This product, called $C_{substrate}$, appears to be a more realistic approach than previous studies that considered all SOC as available carbon.

    At the site level, the SatWetCH4 ~~model~~ calibration reproduces well the boreal fluxes and most of the temperate fluxes, but poorly the emissions seasonality of the tropical sites. This could possibly be improved in future studies by adding high resolution information on local water availability (SWC). Another important improvement would be a calibration per wetland

490 type, which would allow the influence of vegetation to be taken into account as major transport pathways. For this, more eddy covariance flux measurements in the tropics are essential to gain a deeper insight into the processes governing temporal variations in this latitudinal band, and to develop and calibrate this one-step model.

    ~~This~~ SatWetCH4 simple formulation allows fast (within a few seconds) global simulations over decades. ~~Compared to the Global Methane Budget (GMB, Saunois et al. (2020)) LSMs, the SatWetCH4 model shows consistent spatial patterns and~~

495 ~~seasonal variations. However, it is below the range of the GMB LSMs in terms of budget: 86 Tg CH₄ yr⁻¹ (estimated with WAD2M wetland extent) and 70 Tg CH₄ yr⁻¹ (estimated with TOPMODEL wetland extent), while the LSMs show a global range of 102-182 Tg CH₄ yr⁻¹. This underestimation is partly due to the scarcity of eddy covariance data in the tropics, leading to an underrepresentation of high emitting tropical sites.~~, using satellite observations as input data. Although the total methane emission estimates from SatWetCH4 are lower than those reported in the literature (Saunois et al., 2020; McNicol et al., 2023),

500 ~~they are useful~~ SatWetCH4 shows that it is able to reproduce large spatio-temporal variations at 0.25°, which makes it a useful

tool to study methane emissions inter-annual trends. Thus, SatWetCH4 model benefit from independent remote sensing data and from process-based model approach since it is calibrated using in situ site observations.

Finally, we found some inconsistencies in the widely used WAD2M surface wetland extent. A new wetland map is currently being produced (Bernard et al., in prep.), based on GIEMS-2 (Prigent et al., 2020) observations, which provide a seamless estimate of inundated areas with realistic inter-annual variability (Bernard et al., 2024). Applying SatWetCH4 model with this new dataset would allow the study of annual variability and trends in emissions.

Another perspective is the coupling of SatWetCH4 with atmospheric inversions. Indeed, one way to overcome the challenges associated with calibration using surface flux data is to incorporate this simple model into an atmospheric inversion model. This would allow the optimization of both parameters k and Q_{10_0} in the inversion equation using atmospheric concentrations (more numerous than methane fluxes data, especially with satellite data), rather than just the optimization of the methane flux value, as is usually done in inversion models.

Code availability. The optimization and model codes are available at https://doi.org/10.5281/zenodo.11204999.

Data availability. All global forcings used in this study are freely available online: ERA5-Land data at https://cds.climate.copernicus.eu/, WAD2M at https://zenodo.org/records/3998454, TOPMODEL derived wetland extent at https://zenodo.org/records/4571667, and MODIS PsnNet data through https://lpdaac.usgs.gov/products/mod17a2hgfv061/.

Author contributions. J.B., M.S., E.S., P.C., S.P. and A.B. conceived the main ideas of this study and contributed to the research. J.B. built the model, ran the simulations and performed the numerical analyses. J.B. drafted the manuscript with input from M.S. and E.S.. J.B, M.S, E.S P.C., S.P., P.S-O. provided critical feedback on the manuscript. P.G., P.S-C. and J.J. each provided data from a flux tower.

Competing interests. Authors declare no competing interests.

Acknowledgements. J.B. is funded by a PhD grant from the Institut National des Sciences de l'Univers (INSU) of the Centre National de la Recherche Scientifique (CNRS). J.B. would like to thank Vladislav Bastrikov for his insightful help in designing the model calibration. The authors would like to thank the managers of the 55 out of 58 eddy covariance flux towers who made their data available as open source. These data play a crucial role in improving our understanding of methane emissions from wetlands and in calibrating the models more accurately.

References

525 Albuhaisi, Y. A. Y., Van Der Velde, Y., De Jeu, R., Zhang, Z., and Houweling, S.: High-Resolution Estimation of Methane Emissions from Boreal and Pan-Arctic Wetlands Using Advanced Satellite Data, Remote Sensing, 15, 3433, https://doi.org/10.3390/rs15133433, 2023.

Baldocchi, D., Falge, E., Gu, L., Olson, R., Hollinger, D., Running, S., Anthoni, P., Bernhofer, C., Davis, K., Evans, R., Fuentes, J., Goldstein, A., Katul, G., Law, B., Lee, X., Malhi, Y., Meyers, T., Munger, W., Oechel, W., Paw, K. T., Pilegaard, K., Schmid, H. P., Valentini, R., Verma, S., Vesala, T., Wilson, K., and Wofsy, S.: FLUXNET: A New Tool to Study the Temporal and Spatial Variability of Ecosys-
530 tem–Scale Carbon Dioxide, Water Vapor, and Energy Flux Densities, Bulletin of the American Meteorological Society, 82, 2415–2434, https://doi.org/10.1175/1520-0477(2001)082<2415:FANTTS>2.3.CO;2, 2001.

Bernard, J., Prigent, C., Jimenez, C., Frappart, F., Normandin, C., Zeiger, P., Xi, Y., and Peng, S.: Assessing the time variability of GIEMS-2 satellite-derived surface water extent over 30 years, Frontiers in Remote Sensing, 5, https://doi.org/10.3389/frsen.2024.1399234, 2024.

Bloom, A. A., Bowman, K. W., Lee, M., Turner, A. J., Schroeder, R., Worden, J. R., Weidner, R., McDonald, K. C., and Jacob, D. J.: A
535 Global Wetland Methane Emissions and Uncertainty Dataset for Atmospheric Chemical Transport Models (WetCHARTs Version 1.0), Geoscientific Model Development, 10, 2141–2156, https://doi.org/10.5194/gmd-10-2141-2017, 2017.

Bohn, T. J., Melton, J. R., Ito, A., Kleinen, T., Spahni, R., Stocker, B. D., Zhang, B., Zhu, X., Schroeder, R., Glagolev, M. V., Maksyutov, S., Brovkin, V., Chen, G., Denisov, S. N., Eliseev, A. V., Gallego-Sala, A., McDonald, K. C., Rawlins, M., Riley, W. J., Subin, Z. M., Tian, H., Zhuang, Q., and Kaplan, J. O.: WETCHIMP-WSL: Intercomparison of Wetland Methane Emissions Models over West Siberia,
540 Biogeosciences, 12, 3321–3349, https://doi.org/10.5194/bg-12-3321-2015, 2015.

Bridgham, S. D., Cadillo-Quiroz, H., Keller, J. K., and Zhuang, Q.: Methane Emissions from Wetlands: Biogeochemical, Microbial, and Modeling Perspectives from Local to Global Scales, Global Change Biology, 19, 1325–1346, https://doi.org/10.1111/gcb.12131, 2013.

Byrd, R. H., Lu, P., Nocedal, J., and Zhu, C.: A Limited Memory Algorithm for Bound Constrained Optimization, SIAM Journal on Scientific Computing, 16, 1190–1208, https://doi.org/10.1137/0916069, 1995.

545 Chang, K.-Y., Riley, W. J., Knox, S. H., Jackson, R. B., McNicol, G., Poulter, B., Aurela, M., Baldocchi, D., Bansal, S., Bohrer, G., Campbell, D. I., Cescatti, A., Chu, H., Delwiche, K. B., Desai, A. R., Euskirchen, E., Friborg, T., Goeckede, M., Helbig, M., Hemes, K. S., Hirano, T., Iwata, H., Kang, M., Keenan, T., Krauss, K. W., Lohila, A., Mammarella, I., Mitra, B., Miyata, A., Nilsson, M. B., Noormets, A., Oechel, W. C., Papale, D., Peichl, M., Reba, M. L., Rinne, J., Runkle, B. R. K., Ryu, Y., Sachs, T., Schäfer, K. V. R., Schmid, H. P., Shurpali, N., Sonnentag, O., Tang, A. C. I., Torn, M. S., Trotta, C., Tuittila, E.-S., Ueyama, M., Vargas, R., Vesala, T., Windham-Myers, L., Zhang, Z.,
550 and Zona, D.: Substantial Hysteresis in Emergent Temperature Sensitivity of Global Wetland CH4 Emissions, Nature Communications, 12, 2266, https://doi.org/10.1038/s41467-021-22452-1, 2021.

Clymo, R. S., Turunen, J., and Tolonen, K.: Carbon Accumulation in Peatland, Oikos, 81, 368, https://doi.org/10.2307/3547057, 1998.

De Jeu, R. A., Holmes, T. R., Parinussa, R. M., and Owe, M.: A Spatially Coherent Global Soil Moisture Product with Improved Temporal Resolution, Journal of Hydrology, 516, 284–296, https://doi.org/10.1016/j.jhydrol.2014.02.015, 2014.

555 Delwiche, K. B., Knox, S. H., Malhotra, A., Fluet-Chouinard, E., McNicol, G., Feron, S., Ouyang, Z., Papale, D., Trotta, C., Canfora, E., Cheah, Y.-W., Christianson, D., Alberto, M. C. R., Alekseychik, P., Aurela, M., Baldocchi, D., Bansal, S., Billesbach, D. P., Bohrer, G., Bracho, R., Buchmann, N., Campbell, D. I., Celis, G., Chen, J., Chen, W., Chu, H., Dalmagro, H. J., Dengel, S., Desai, A. R., Detto, M., Dolman, H., Eichelmann, E., Euskirchen, E., Famulari, D., Friborg, T., Fuchs, K., Goeckede, M., Gogo, S., Gondwe, M. J., Goodrich, J. P., Gottschalk, P., Graham, S. L., Heimann, M., Helbig, M., Helfter, C., Hemes, K. S., Hirano, T., Hollinger, D., Hörtnagl, L., Iwata,
560 H., Jacotot, A., Jansen, J., Jurasinski, G., Kang, M., Kasak, K., King, J., Klatt, J., Koebsch, F., Krauss, K. W., Lai, D. Y. F., Mammarella,

I., Manca, G., Marchesini, L. B., Matthes, J. H., Maximon, T., Merbold, L., Mitra, B., Morin, T. H., Nemitz, E., Nilsson, M. B., Niu, S., Oechel, W. C., Oikawa, P. Y., Ono, K., Peichl, M., Peltola, O., Reba, M. L., Richardson, A. D., Riley, W., Runkle, B. R. K., Ryu, Y., Sachs, T., Sakabe, A., Sanchez, C. R., Schuur, E. A., Schäfer, K. V. R., Sonnentag, O., Sparks, J. P., Stuart-Haëntjens, E., Sturtevant, C., Sullivan, R. C., Szutu, D. J., Thom, J. E., Torn, M. S., Tuittila, E.-S., Turner, J., Ueyama, M., Valach, A. C., Vargas, R., Varlagin, A., Vazquez-Lule, A., Verfaillie, J. G., Vesala, T., Vourlitis, G. L., Ward, E. J., Wille, C., Wohlfahrt, G., Wong, G. X., Zhang, Z., Zona, D., Windham-Myers, L., Poulter, B., and Jackson, R. B.: FLUXNET-CH4: A Global, Multi-Ecosystem Dataset and Analysis of Methane Seasonality from Freshwater Wetlands, Preprint, Biosphere – Biogeosciences, https://doi.org/10.5194/essd-2020-307, 2021.

Denny, P.: Biodiversity and Wetlands, Wetlands Ecology and Management, 3, https://doi.org/10.1007/BF00177296, 1994.

England, M. R., Eisenman, I., Lutsko, N. J., and Wagner, T. J. W.: The Recent Emergence of Arctic Amplification, Geophysical Research Letters, 48, e2021GL094 086, https://doi.org/10.1029/2021GL094086, 2021.

Fan, Y., Li, H., and Miguez-Macho, G.: Global Patterns of Groundwater Table Depth, Science, 339, 940–943, https://doi.org/10.1126/science.1229881, 2013.

Feron, S., Malhotra, A., Bansal, S., Fluet-Chouinard, E., McNicol, G., Knox, S. H., Delwiche, K. B., Cordero, R. R., Ouyang, Z., Zhang, Z., Poulter, B., and Jackson, R. B.: Recent Increases in Annual, Seasonal, and Extreme Methane Fluxes Driven by Changes in Climate and Vegetation in Boreal and Temperate Wetland Ecosystems, Global Change Biology, 30, e17 131, https://doi.org/10.1111/gcb.17131, 2024.

Forster, P., Storelvmo, T., Armour, K., Collins, W., Dufresne, J.-L., Frame, D., Lunt, D., Mauritsen, T., Palmer, M., Watanabe, M., Wild, M., and Zhang, H.: The Earth's Energy Budget, Climate Feedbacks, and Climate Sensitivity, p. 923–1054, Cambridge University Press, Cambridge, United Kingdom and New York, NY, USA, https://doi.org/10.1017/9781009157896.009, 2021.

Ge, M., Korrensalo, A., Laiho, R., Kohl, L., Lohila, A., Pihlatie, M., Li, X., Laine, A. M., Anttila, J., Putkinen, A., Wang, W., and Koskinen, M.: Plant-Mediated CH4 Exchange in Wetlands: A Review of Mechanisms and Measurement Methods with Implications for Modelling, Science of The Total Environment, 914, 169 662, https://doi.org/10.1016/j.scitotenv.2023.169662, 2024.

Gedney, N.: Climate Feedback from Wetland Methane Emissions, Geophysical Research Letters, 31, L20 503, https://doi.org/10.1029/2004GL020919, 2004.

Gedney, N. and Cox, P. M.: The Sensitivity of Global Climate Model Simulations to the Representation of Soil Moisture Heterogeneity, Journal of Hydrometeorology, 4, 1265–1275, https://doi.org/10.1175/1525-7541(2003)004<1265:TSOGCM>2.0.CO;2, 2003.

Gedney, N., Huntingford, C., Comyn-Platt, E., and Wiltshire, A.: Significant Feedbacks of Wetland Methane Release on Climate Change and the Causes of Their Uncertainty, Environmental Research Letters, 14, 084 027, https://doi.org/10.1088/1748-9326/ab2726, 2019.

Gordon, C., Gregory, J. M., and Wood, R. A.: The Simulation of SST, Sea Ice Extents and Ocean Heat Transports in a Version of the Hadley Centre Coupled Model without ⁻ux Adjustments, Clim. Dyn., 2000.

Guimberteau, M., Zhu, D., Maignan, F., Huang, Y., Yue, C., Dantec-Nédélec, S., Ottlé, C., Jornet-Puig, A., Bastos, A., Laurent, P., Goll, D., Bowring, S., Chang, J., Guenet, B., Tifafi, M., Peng, S., Krinner, G., Ducharne, A., Wang, F., Wang, T., Wang, X., Wang, Y., Yin, Z., Lauerwald, R., Joetzjer, E., Qiu, C., Kim, H., and Ciais, P.: ORCHIDEE-MICT (v8.4.1), a Land Surface Model for the High Latitudes: Model Description and Validation, Geoscientific Model Development, 11, 121–163, https://doi.org/10.5194/gmd-11-121-2018, 2018.

Hengl, T., Mendes de Jesus, J., Heuvelink, G. B. M., Ruiperez Gonzalez, M., Kilibarda, M., Blagotić, A., Shangguan, W., Wright, M. N., Geng, X., Bauer-Marschallinger, B., Guevara, M. A., Vargas, R., MacMillan, R. A., Batjes, N. H., Leenaars, J. G. B., Ribeiro, E., Wheeler, I., Mantel, S., and Kempen, B.: SoilGrids250m: Global Gridded Soil Information Based on Machine Learning, PLOS ONE, 12, e0169 748, https://doi.org/10.1371/journal.pone.0169748, 2017.

Jackson, R. B., Saunois, M., Bousquet, P., Canadell, J. G., Poulter, B., Stavert, A. R., Bergamaschi, P., Niwa, Y., Segers, A., and Tsuruta, A.: Increasing Anthropogenic Methane Emissions Arise Equally from Agricultural and Fossil Fuel Sources, Environmental Research Letters, 15, 071 002, https://doi.org/10.1088/1748-9326/ab9ed2, 2020.

Jensen, K. and Mcdonald, K.: Surface Water Microwave Product Series Version 3: A Near-Real Time and 25-Year Historical Global Inundated Area Fraction Time Series From Active and Passive Microwave Remote Sensing, IEEE Geoscience and Remote Sensing Letters, 16, 1402–1406, https://doi.org/10.1109/LGRS.2019.2898779, 2019.

Khvorostyanov, D. V., Krinner, G., Ciais, P., Heimann, M., and Zimov, S. A.: Vulnerability of Permafrost Carbon to Global Warming. Part I: Model Description and Role of Heat Generated by Organic Matter Decomposition, Tellus B: Chemical and Physical Meteorology, 60, 250, https://doi.org/10.1111/j.1600-0889.2007.00333.x, 2008.

Knox, S. H., Bansal, S., McNicol, G., Schafer, K., Sturtevant, C., Ueyama, M., Valach, A. C., Baldocchi, D., Delwiche, K., Desai, A. R., Euskirchen, E., Liu, J., Lohila, A., Malhotra, A., Melling, L., Riley, W., Runkle, B. R. K., Turner, J., Vargas, R., Zhu, Q., Alto, T., Fluet-Chouinard, E., Goeckede, M., Melton, J. R., Sonnentag, O., Vesala, T., Ward, E., Zhang, Z., Feron, S., Ouyang, Z., Alekseychik, P., Aurela, M., Bohrer, G., Campbell, D. I., Chen, J., Chu, H., Dalmagro, H. J., Goodrich, J. P., Gottschalk, P., Hirano, T., Iwata, H., Jurasinski, G., Kang, M., Koebsch, F., Mammarella, I., Nilsson, M. B., Ono, K., Peichl, M., Peltola, O., Ryu, Y., Sachs, T., Sakabe, A., Sparks, J. P., Tuittila, E.-S., Vourlitis, G. L., Wong, G. X., Windham-Myers, L., Poulter, B., and Jackson, R. B.: Identifying Dominant Environmental Predictors of Freshwater Wetland Methane Fluxes across Diurnal to Seasonal Time Scales, Global Change Biology, 27, 3582–3604, https://doi.org/10.1111/gcb.15661, 2021.

Kuhn, M. A., Varner, R. K., Bastviken, D., Crill, P., MacIntyre, S., Turetsky, M., Walter Anthony, K., McGuire, A. D., and Olefeldt, D.: BAWLD-CH$_4$: A Comprehensive Dataset of Methane Fluxes from Boreal and Arctic Ecosystems, Earth System Science Data, 13, 5151–5189, https://doi.org/10.5194/essd-13-5151-2021, 2021.

Kumar, A., Bhatia, A., Fagodiya, RK., Malyan, SK., and Meena, BL.: Eddy Covariance Flux Tower: A Promising Technique for Greenhouse Gases Measurement, Advances in Plants & Agriculture Research, 7, https://doi.org/10.15406/apar.2017.07.00263, 2017.

McNicol, G., Fluet-Chouinard, E., Ouyang, Z., Knox, S., Zhang, Z., Aalto, T., Bansal, S., Chang, K.-Y., Chen, M., Delwiche, K., Feron, S., Goeckede, M., Liu, J., Malhotra, A., Melton, J. R., Riley, W., Vargas, R., Yuan, K., Ying, Q., Zhu, Q., Alekseychik, P., Aurela, M., Billesbach, D. P., Campbell, D. I., Chen, J., Chu, H., Desai, A. R., Euskirchen, E., Goodrich, J., Griffis, T., Helbig, M., Hirano, T., Iwata, H., Jurasinski, G., King, J., Koebsch, F., Kolka, R., Krauss, K., Lohila, A., Mammarella, I., Nilson, M., Noormets, A., Oechel, W., Peichl, M., Sachs, T., Sakabe, A., Schulze, C., Sonnentag, O., Sullivan, R. C., Tuittila, E.-S., Ueyama, M., Vesala, T., Ward, E., Wille, C., Wong, G. X., Zona, D., Windham-Myers, L., Poulter, B., and Jackson, R. B.: Upscaling Wetland Methane Emissions From the FLUXNET-CH4 Eddy Covariance Network (UpCH4 v1.0): Model Development, Network Assessment, and Budget Comparison, AGU Advances, 4, e2023AV000 956, https://doi.org/10.1029/2023AV000956, 2023.

Meli, P., Rey Benayas, J. M., Balvanera, P., and Martínez Ramos, M.: Restoration Enhances Wetland Biodiversity and Ecosystem Service Supply, but Results Are Context-Dependent: A Meta-Analysis, PLoS ONE, 9, e93 507, https://doi.org/10.1371/journal.pone.0093507, 2014.

Melton, J. R., Wania, R., Hodson, E. L., Poulter, B., Ringeval, B., Spahni, R., Bohn, T., Avis, C. A., Beerling, D. J., Chen, G., Eliseev, A. V., Denisov, S. N., Hopcroft, P. O., Lettenmaier, D. P., Riley, W. J., Singarayer, J. S., Subin, Z. M., Tian, H., Zürcher, S., Brovkin, V., van Bodegom, P. M., Kleinen, T., Yu, Z. C., and Kaplan, J. O.: Present State of Global Wetland Extent and Wetland Methane Modelling: Conclusions from a Model Inter-Comparison Project (WETCHIMP), Biogeosciences, 10, 753–788, https://doi.org/10.5194/bg-10-753-2013, 2013.

Meng, L., Paudel, R., Hess, P. G. M., and Mahowald, N. M.: Seasonal and Interannual Variability in Wetland Methane Emissions Simulated by CLM4Me' and CAM-chem and Comparisons to Observations of Concentrations, Biogeosciences, 12, 4029–4049, https://doi.org/10.5194/bg-12-4029-2015, 2015.

Morel, X., Decharme, B., Delire, C., Krinner, G., Lund, M., Hansen, B. U., and Mastepanov, M.: A New Process-Based Soil Methane Scheme: Evaluation Over Arctic Field Sites With the ISBA Land Surface Model, Journal of Advances in Modeling Earth Systems, 11, 293–326, https://doi.org/10.1029/2018MS001329, 2019.

Muñoz-Sabater, J., Dutra, E., Agustí-Panareda, A., Albergel, C., Arduini, G., Balsamo, G., Boussetta, S., Choulga, M., Harrigan, S., Hersbach, H., Martens, B., Miralles, D. G., Piles, M., Rodríguez-Fernández, N. J., Zsoter, E., Buontempo, C., and Thépaut, J.-N.: ERA5-Land: A State-of-the-Art Global Reanalysis Dataset for Land Applications, Earth System Science Data, 13, 4349–4383, https://doi.org/10.5194/essd-13-4349-2021, 2021.

Nzotungicimpaye, C.-M., Zickfeld, K., MacDougall, A. H., Melton, J. R., Treat, C. C., Eby, M., and Lesack, L. F. W.: WETMETH 1.0: A New Wetland Methane Model for Implementation in Earth System Models, Geoscientific Model Development, 14, 6215–6240, https://doi.org/10.5194/gmd-14-6215-2021, 2021.

Parton, W. J., Schimel, D. S., Cole, C. V., and Ojima, D. S.: Analysis of Factors Controlling Soil Organic Matter Levels in Great Plains Grasslands, Soil Science Society of America Journal, 51, 1173–1179, https://doi.org/10.2136/sssaj1987.03615995005100050015x, 1987.

Peltola, O., Vesala, T., Gao, Y., Räty, O., Alekseychik, P., Aurela, M., Chojnicki, B., Desai, A. R., Dolman, A. J., Euskirchen, E. S., Friborg, T., Göckede, M., Helbig, M., Humphreys, E., Jackson, R. B., Jocher, G., Joos, F., Klatt, J., Knox, S. H., Kowalska, N., Kutzbach, L., Lienert, S., Lohila, A., Mammarella, I., Nadeau, D. F., Nilsson, M. B., Oechel, W. C., Peichl, M., Pypker, T., Quinton, W., Rinne, J., Sachs, T., Samson, M., Schmid, H. P., Sonnentag, O., Wille, C., Zona, D., and Aalto, T.: Monthly Gridded Data Product of Northern Wetland Methane Emissions Based on Upscaling Eddy Covariance Observations, Earth System Science Data, 11, 1263–1289, https://doi.org/10.5194/essd-11-1263-2019, 2019.

Pham-Duc, B., Prigent, C., Aires, F., and Papa, F.: Comparisons of Global Terrestrial Surface Water Datasets over 15 Years, Journal of Hydrometeorology, 18, 993–1007, https://doi.org/10.1175/JHM-D-16-0206.1, 2017.

Post, E., Alley, R. B., Christensen, T. R., Macias-Fauria, M., Forbes, B. C., Gooseff, M. N., Iler, A., Kerby, J. T., Laidre, K. L., Mann, M. E., Olofsson, J., Stroeve, J. C., Ulmer, F., Virginia, R. A., and Wang, M.: The Polar Regions in a 2°C Warmer World, Science Advances, 5, eaaw9883, https://doi.org/10.1126/sciadv.aaw9883, 2019.

Poulter, B., Fluet-Chouinard, E., Hugelius, G., Koven, C., Fatoyinbo, L., Page, S. E., Rosentreter, J. A., Smart, L. S., Taillie, P. J., Thomas, N., Zhang, Z., and Wijedasa, L. S.: A Review of Global Wetland Carbon Stocks and Management Challenges, in: Geophysical Monograph Series, edited by Krauss, K. W., Zhu, Z., and Stagg, C. L., pp. 1–20, Wiley, 1 edn., https://doi.org/10.1002/9781119639305.ch1, 2021.

Previdi, M., Smith, K. L., and Polvani, L. M.: Arctic Amplification of Climate Change: A Review of Underlying Mechanisms, Environmental Research Letters, 16, 093 003, https://doi.org/10.1088/1748-9326/ac1c29, 2021.

Prigent, C., Jimenez, C., and Bousquet, P.: Satellite-Derived Global Surface Water Extent and Dynamics Over the Last 25 Years (GIEMS-2), Journal of Geophysical Research: Atmospheres, 125, https://doi.org/10.1029/2019JD030711, 2020.

Qiu, C., Zhu, D., Ciais, P., Guenet, B., Peng, S., Krinner, G., Tootchi, A., Ducharne, A., and Hastie, A.: Modelling Northern Peatland Area and Carbon Dynamics since the Holocene with the ORCHIDEE-PEAT Land Surface Model (SVN R5488), Geoscientific Model Development, 12, 2961–2982, https://doi.org/10.5194/gmd-12-2961-2019, 2019.

Riley, W. J., Subin, Z. M., Lawrence, D. M., Swenson, S. C., Torn, M. S., Meng, L., Mahowald, N. M., and Hess, P.: Barriers to Predicting Changes in Global Terrestrial Methane Fluxes: Analyses Using CLM4Me, a Methane Biogeochemistry Model Integrated in CESM, Biogeosciences, 8, 1925–1953, https://doi.org/10.5194/bg-8-1925-2011, 2011.

675 Ringeval, B., de Noblet-Ducoudré, N., Ciais, P., Bousquet, P., Prigent, C., Papa, F., and Rossow, W. B.: An Attempt to Quantify the Impact of Changes in Wetland Extent on Methane Emissions on the Seasonal and Interannual Time Scales: WETLAND EXTENT'S CHANGES AND CH $_4$ EMISSIONS, Global Biogeochemical Cycles, 24, n/a–n/a, https://doi.org/10.1029/2008GB003354, 2010.

Rößger, N., Sachs, T., Wille, C., Boike, J., and Kutzbach, L.: Seasonal Increase of Methane Emissions Linked to Warming in Siberian Tundra, Nature Climate Change, 12, 1031–1036, https://doi.org/10.1038/s41558-022-01512-4, 2022.

680 Running, S. W. and Zhao, M.: Daily GPP and Annual NPP (MOD17A2H/A3H) and Year-end Gap- Filled (MOD17A2HGF/A3HGF) Products NASA Earth Observing System MODIS Land Algorithm (For Collection 6.1), 2021.

Salmon, E., Jégou, F., Guenet, B., Jourdain, L., Qiu, C., Bastrikov, V., Guimbaud, C., Zhu, D., Ciais, P., Peylin, P., Gogo, S., Laggoun-Défarge, F., Aurela, M., Bret-Harte, M. S., Chen, J., Chojnicki, B. H., Chu, H., Edgar, C. W., Euskirchen, E. S., Flanagan, L. B., Fortuniak, K., Holl, D., Klatt, J., Kolle, O., Kowalska, N., Kutzbach, L., Lohila, A., Merbold, L., Pawlak, W., Sachs, T., and Ziemblińska, K.: Assessing
685 Methane Emissions for Northern Peatlands in ORCHIDEE-PEAT Revision 7020, Geoscientific Model Development, 15, 2813–2838, https://doi.org/10.5194/gmd-15-2813-2022, 2022.

Saunois, M., Bousquet, P., Poulter, B., Peregon, A., Ciais, P., Canadell, J. G., Dlugokencky, E. J., Etiope, G., Bastviken, D., Houweling, S., Janssens-Maenhout, G., Tubiello, F. N., Castaldi, S., Jackson, R. B., Alexe, M., Arora, V. K., Beerling, D. J., Bergamaschi, P., Blake, D. R., Brailsford, G., Brovkin, V., Bruhwiler, L., Crevoisier, C., Crill, P., Covey, K., Curry, C., Frankenberg, C., Gedney, N., Höglund-Isaksson,
690 L., Ishizawa, M., Ito, A., Joos, F., Kim, H.-S., Kleinen, T., Krummel, P., Lamarque, J.-F., Langenfelds, R., Locatelli, R., Machida, T., Maksyutov, S., McDonald, K. C., Marshall, J., Melton, J. R., Morino, I., Naik, V., O'Doherty, S., Parmentier, F.-J. W., Patra, P. K., Peng, C., Peng, S., Peters, G. P., Pison, I., Prigent, C., Prinn, R., Ramonet, M., Riley, W. J., Saito, M., Santini, M., Schroeder, R., Simpson, I. J., Spahni, R., Steele, P., Takizawa, A., Thornton, B. F., Tian, H., Tohjima, Y., Viovy, N., Voulgarakis, A., van Weele, M., van der Werf, G. R., Weiss, R., Wiedinmyer, C., Wilton, D. J., Wiltshire, A., Worthy, D., Wunch, D., Xu, X., Yoshida, Y., Zhang, B., Zhang, Z., and Zhu, Q.:
695 The Global Methane Budget 2000–2012, Earth System Science Data, 8, 697–751, https://doi.org/10.5194/essd-8-697-2016, 2016.

Saunois, M., Stavert, A. R., Poulter, B., Bousquet, P., Canadell, J. G., Jackson, R. B., Raymond, P. A., Dlugokencky, E. J., Houweling, S., Patra, P. K., Ciais, P., Arora, V. K., Bastviken, D., Bergamaschi, P., Blake, D. R., Brailsford, G., Bruhwiler, L., Carlson, K. M., Carrol, M., Castaldi, S., Chandra, N., Crevoisier, C., Crill, P. M., Covey, K., Curry, C. L., Etiope, G., Frankenberg, C., Gedney, N., Hegglin, M. I., Höglund-Isaksson, L., Hugelius, G., Ishizawa, M., Ito, A., Janssens-Maenhout, G., Jensen, K. M., Joos, F., Kleinen, T., Krummel,
700 P. B., Langenfelds, R. L., Laruelle, G. G., Liu, L., Machida, T., Maksyutov, S., McDonald, K. C., McNorton, J., Miller, P. A., Melton, J. R., Morino, I., Müller, J., Murguia-Flores, F., Naik, V., Niwa, Y., Noce, S., O'Doherty, S., Parker, R. J., Peng, C., Peng, S., Peters, G. P., Prigent, C., Prinn, R., Ramonet, M., Regnier, P., Riley, W. J., Rosentreter, J. A., Segers, A., Simpson, I. J., Shi, H., Smith, S. J., Steele, L. P., Thornton, B. F., Tian, H., Tohjima, Y., Tubiello, F. N., Tsuruta, A., Viovy, N., Voulgarakis, A., Weber, T. S., van Weele, M., van der Werf, G. R., Weiss, R. F., Worthy, D., Wunch, D., Yin, Y., Yoshida, Y., Zhang, W., Zhang, Z., Zhao, Y., Zheng, B., Zhu, Q., Zhu, Q., and Zhuang,
705 Q.: The Global Methane Budget 2000–2017, Earth System Science Data, 12, 1561–1623, https://doi.org/10.5194/essd-12-1561-2020, 2020.

Schädel, C., Schuur, E. A. G., Bracho, R., Elberling, B., Knoblauch, C., Lee, H., Luo, Y., Shaver, G. R., and Turetsky, M. R.: Circumpolar Assessment of Permafrost C Quality and Its Vulnerability over Time Using Long-Term Incubation Data, Global Change Biology, 20, 641–652, https://doi.org/10.1111/gcb.12417, 2014.

710 Schuur, E. A., Abbott, B. W., Commane, R., Ernakovich, J., Euskirchen, E., Hugelius, G., Grosse, G., Jones, M., Koven, C., Leshyk, V., Lawrence, D., Loranty, M. M., Mauritz, M., Olefeldt, D., Natali, S., Rodenhizer, H., Salmon, V., Schädel, C., Strauss, J., Treat, C., and Turetsky, M.: Permafrost and Climate Change: Carbon Cycle Feedbacks From the Warming Arctic, Annual Review of Environment and Resources, 47, 343–371, https://doi.org/10.1146/annurev-environ-012220-011847, 2022.

Tenkanen, M., Tsuruta, A., Rautiainen, K., Kangasaho, V., Ellul, R., and Aalto, T.: Utilizing Earth Observations of Soil Freeze/Thaw Data
715 and Atmospheric Concentrations to Estimate Cold Season Methane Emissions in the Northern High Latitudes, Remote Sensing, 13, 5059, https://doi.org/10.3390/rs13245059, 2021.

Torres-Alvarado, R., Ramírez-Vives, F., and Fernández, F. J.: Methanogenesis and Methane Oxidation in Wetlands. Implications in the Global Carbon Cycle Metanogénesis y Metano-Oxidación En Humedales. Implicaciones En El Ciclo Del Carbono Global, Hidrobiológica, 15, 2005.

720 Ueyama, M., Knox, S. H., Delwiche, K. B., Bansal, S., Riley, W. J., Baldocchi, D., Hirano, T., McNicol, G., Schafer, K., Windham-Myers, L., Poulter, B., Jackson, R. B., Chang, K.-Y., Chen, J., Chu, H., Desai, A. R., Gogo, S., Iwata, H., Kang, M., Mammarella, I., Peichl, M., Sonnentag, O., Tuittila, E.-S., Ryu, Y., Euskirchen, E. S., Göckede, M., Jacotot, A., Nilsson, M. B., and Sachs, T.: Modeled Production, Oxidation, and Transport Processes of Wetland Methane Emissions in Temperate, Boreal, and Arctic Regions, Global Change Biology, 29, 2313–2334, https://doi.org/10.1111/gcb.16594, 2023.

725 Valentini, R.: Fluxes of Carbon, Water and Energy of European Forests, Springer Berlin Heidelberg, https://doi.org/10.1007/978-3-662-05171-9, 2003.

Walter, B. P. and Heimann, M.: A Process-Based, Climate-Sensitive Model to Derive Methane Emissions from Natural Wetlands: Application to Five Wetland Sites, Sensitivity to Model Parameters, and Climate, Global Biogeochemical Cycles, 14, 745–765, https://doi.org/10.1029/1999GB001204, 2000.

730 Wania, R., Melton, J. R., Hodson, E. L., Poulter, B., Ringeval, B., Spahni, R., Bohn, T., Avis, C. A., Chen, G., Eliseev, A. V., Hopcroft, P. O., Riley, W. J., Subin, Z. M., Tian, H., van Bodegom, P. M., Kleinen, T., Yu, Z. C., Singarayer, J. S., Zürcher, S., Lettenmaier, D. P., Beerling, D. J., Denisov, S. N., Prigent, C., Papa, F., and Kaplan, J. O.: Present State of Global Wetland Extent and Wetland Methane Modelling: Methodology of a Model Inter-Comparison Project (WETCHIMP), Geoscientific Model Development, 6, 617–641, https://doi.org/10.5194/gmd-6-617-2013, 2013.

735 Wieder, W.: Regridded Harmonized World Soil Database v1.2, https://doi.org/10.3334/ORNLDAAC/1247, 2014.

Xi, Y., Peng, S., Ducharne, A., Ciais, P., Gumbricht, T., Jimenez, C., Poulter, B., Prigent, C., Qiu, C., Saunois, M., and Zhang, Z.: Dynamics of global wetlands by TOPMODEL, https://doi.org/10.5281/ZENODO.6409309, 2021.

Xi, Y., Peng, S., Ducharne, A., Ciais, P., Gumbricht, T., Jimenez, C., Poulter, B., Prigent, C., Qiu, C., Saunois, M., and Zhang, Z.: Gridded Maps of Wetlands Dynamics over Mid-Low Latitudes for 1980–2020 Based on TOPMODEL, Scientific Data, 9, 347,
740 https://doi.org/10.1038/s41597-022-01460-w, 2022.

Xu, J., Morris, P. J., Liu, J., and Holden, J.: PEATMAP: Refining Estimates of Global Peatland Distribution Based on a Meta-Analysis, CATENA, 160, 134–140, https://doi.org/10.1016/j.catena.2017.09.010, 2018.

Zhang, Y., Xiao, X., Wu, X., Zhou, S., Zhang, G., Qin, Y., and Dong, J.: A Global Moderate Resolution Dataset of Gross Primary Production of Vegetation for 2000–2016, Scientific Data, 4, 170 165, https://doi.org/10.1038/sdata.2017.165, 2017.

745 Zhang, Z., Fluet-Chouinard, E., Jensen, K., McDonald, K., Hugelius, G., Gumbricht, T., Carroll, M., Prigent, C., Bartsch, A., and Poulter, B.: Development of a global dataset of Wetland Area and Dynamics for Methane Modeling (WAD2M), https://doi.org/10.5281/ZENODO.5553187, 2021a.

Zhang, Z., Fluet-Chouinard, E., Jensen, K., McDonald, K., Hugelius, G., Gumbricht, T., Carroll, M., Prigent, C., Bartsch, A., and Poulter, B.: Development of the Global Dataset of Wetland Area and Dynamics for Methane Modeling (WAD2M), Earth System Science Data, 13, 2001–2023, https://doi.org/10.5194/essd-13-2001-2021, 2021b.

Zhu, X., Zhuang, Q., Qin, Z., Glagolev, M., and Song, L.: Estimating Wetland Methane Emissions from the Northern High Latitudes from 1990 to 2009 Using Artificial Neural Networks: METHANE EMISSIONS FROM NORTHERN WETLANDS, Global Biogeochemical Cycles, 27, 592–604, https://doi.org/10.1002/gbc.20052, 2013.

750

Supplementary material of Satellite-based modeling of wetland methane emissions on a global scale (SatWetCH4 1.0)

Juliette Bernard[1,2], Elodie Salmon[1], Marielle Saunois[1], Shushi Peng[3], Penélope Serrano-Ortiz[4], Antoine Berchet[1], Palingamoorthy Gnanamoorthy[5,6], Joachim Jansen[7], and Philippe Ciais[1]

[1]Laboratoire des Sciences du Climat et de l'Environnement, CEA-CNRS-UVSQ, Gif-sur-Yvette, France
[2]LERMA, Paris Observatory, CNRS, PSL, Paris, France
[3]College of Urban and Environmental Sciences, Peking University, Beijing 100871, China
[4]Department of Ecology, Andalusian Institute for Earth System Research (CEAMA-IISTA), University of Granada, Spain
[5]CAS Key Laboratory of Tropical Forest Ecology, Xishuangbanna Tropical Botanical Garden, Chinese Academy of Sciences, Menglun, China
[6]Coastal Systems Research, M. S. Swaminathan Research Foundation, Chennai, India
[7]Department of Ecology and Genetics/Limnology, Uppsala University, Uppsala, Sweden

Correspondence: Juliette Bernard (juliette.bernard@obspm.fr)

A Information about in situ fluxes and ancillary data

Table S1. Methane eddy covariance flux data sources

Source	Data access	Accessed
FLUX-NET CH4	https://fluxnet.org/data/fluxnet-ch4-community-product/	1^{rst} August 2022
AmeriFlux	https://ameriflux.lbl.gov/sites/site-search/	3rd October 2022
EuroFlux	http://www.europe-fluxdata.eu/home/data/request-data	Novembre 2022
P. Gnanamoorthy	Personal exchanges	29th Octobre 2022
C. Helfter	https://catalogue.ceh.ac.uk/documents/d366ed40-af8c-42be-86f2-bb90b11a659e https://catalogue.ceh.ac.uk/documents/2170ebd0-7e6f-4871-97d9-1d42e210468f	10th October 2022

Table S2: List of methane eddy covariance flux sites used in this study

site ID	data source	lat	lon	start	end	monthly data	DOI
US-A10	FLUXNET	71.3	-156.6	2012	2018	21	https://doi.org/10.18140/FLX/1669662
US-Beo	FLUXNET	71.3	-156.6	2013	2014	16	No DOI available
US-Bes	FLUXNET	71.3	-156.6	2013	2015	27	No DOI available
US-NGB	FLUXNET	71.3	-156.6	2012	2018	39	https://doi.org/10.18140/FLX/1669687
RU-Cok	FLUXNET	70.8	147.5	2008	2016	21	https://doi.org/10.18140/FLX/1669656
US-A03	FLUXNET	70.5	-149.9	2015	2018	28	https://doi.org/10.18140/FLX/1669661
US-Atq	FLUXNET	70.5	-157.4	2013	2016	27	https://doi.org/10.18140/FLX/1669663
RU-Ch2	FLUXNET	68.6	161.4	2014	2016	26	https://doi.org/10.18140/FLX/1669654
US-ICs	AmeriFlux	68.6	-149.3	2007	2021	52	https://doi.org/10.17190/AMF/1246130
US-Ivo	FLUXNET	68.5	-155.8	2013	2016	41	https://doi.org/10.18140/FLX/1669679
SE-St1	EuroFlux	68.4	19.1	2012	2019	70	No DOI available
FI-Lom	FLUXNET	68	24.2	2006	2010	60	https://doi.org/10.18140/FLX/1669638
US-Uaf	FLUXNET	64.9	-147.9	2011	2018	48	https://doi.org/10.18140/FLX/1669701
US-NGC	FLUXNET	64.9	-163.7	2017	2018	8	https://doi.org/10.18140/FLX/1669688
US-BZF	AmeriFlux	64.7	-148.3	2011	2022	56	https://doi.org/10.17190/AMF/1756433

US-BZB	AmeriFlux	64.7	-148.3	2011	2022	59	https://doi.org/10.17190/AMF/1773401
US-BZo	AmeriFlux	64.7	-148.3	2018	2022	30	https://doi.org/10.17190/AMF/1846662
SE-Deg	EuroFlux	64.2	19.6	2014	2020	76	No DOI available
FI-Si2	FLUXNET	61.8	24.2	2012	2016	34	https://doi.org/10.18140/FLX/1669639
FI-Sii	EuroFlux	61.8	24.2	2008	2020	130	No DOI available
CA-SCB	FLUXNET	61.3	-121.3	2014	2017	30	https://doi.org/10.18140/FLX/1669613
US-KPL	AmeriFlux	60.5	-150.5	2021	2021	7	https://doi.org/10.17190/AMF/1865478
DE-Hte	FLUXNET	54.2	12.2	2011	2018	85	https://doi.org/10.18140/FLX/1669634
DE-Zrk	FLUXNET	53.9	12.9	2013	2018	63	https://doi.org/10.18140/FLX/1669636
DE-UtM	EuroFlux	52.5	8.8	2016	2017	19	No DOI available
CA-DBB	AmeriFlux	49.1	-123	2014	2020	58	https://doi.org/10.17190/AMF/1543378
CA-DB2	AmeriFlux	49.1	-123	2019	2020	13	https://doi.org/10.17190/AMF/1881564
DE-SfN	FLUXNET	47.8	11.1	2012	2014	29	https://doi.org/10.18140/FLX/1669635
US-Los	AmeriFlux	46.1	-90	2000	2022	91	https://doi.org/10.17190/AMF/1246071
US-ALQ	AmeriFlux	46	-89.6	2015	2022	35	https://doi.org/10.17190/AMF/1480323
JP-BBY	FLUXNET	43.3	141.8	2015	2018	40	https://doi.org/10.18140/FLX/1669646
US-WPT	FLUXNET	41.5	-83	2011	2013	34	https://doi.org/10.18140/FLX/1669702
US-MRM	FLUXNET	40.8	-74	2012	2013	21	No DOI available
US-ORv	FLUXNET	40	-83	2011	2015	50	https://doi.org/10.18140/FLX/1669689
US-StJ	AmeriFlux	39.1	-75.4	2014	2017	31	https://doi.org/10.17190/AMF/1480316
US-Hsm	AmeriFlux	38.2	-122	2021	2022	10	https://doi.org/10.17190/AMF/1890483
US-Srr	FLUXNET	38.2	-122	2014	2017	43	https://doi.org/10.18140/FLX/1669694
US-Tw1	AmeriFlux	38.1	-121.6	2011	2020	115	https://doi.org/10.17190/AMF/1246147
US-Tw5	AmeriFlux	38.1	-121.6	2018	2020	22	https://doi.org/10.17190/AMF/1543380
US-Tw4	AmeriFlux	38.1	-121.6	2013	2021	93	https://doi.org/10.17190/AMF/1246151
US-Myb	AmeriFlux	38	-121.8	2010	2021	133	https://doi.org/10.17190/AMF/1246139
US-Sne	FLUXNET	38	-121.8	2016	2018	32	https://doi.org/10.18140/FLX/1669693
US-EDN	AmeriFlux	37.6	-122.1	2018	2019	20	https://doi.org/10.17190/AMF/1543381
ES-Pdu	EuroFlux	37	-3.6	2014	2017	38	https://doi.org/10.1029/2019JG005169
US-NC4	AmeriFlux	35.8	-75.9	2009	2021	39	https://doi.org/10.17190/AMF/1480314
US-HB1	AmeriFlux	33.3	-79.2	2019	2021	12	https://doi.org/10.17190/AMF/1660341
US-LA2	FLUXNET	29.9	-90.3	2011	2013	22	https://doi.org/10.18140/FLX/1669681
US-LA1	FLUXNET	29.5	-90.4	2011	2012	15	https://doi.org/10.18140/FLX/1669680

US-DPW	FLUXNET	28.1	-81.4	2013	2017	40	https://doi.org/10.18140/FLX/1669672
HK-MPM	FLUXNET	22.5	114	2016	2018	34	https://doi.org/10.18140/FLX/1669642
IN-Pic	P. Gnanamoorthy	11.4	79.8	2018	2020	8	No DOI available
MY-MLM	FLUXNET	1.5	111.1	2014	2015	19	https://doi.org/10.18140/FLX/1669650
ID-Pag	FLUXNET	-2.3	113.9	2016	2017	12	https://doi.org/10.18140/FLX/1669643
PE-QFR	AmeriFlux	-3.8	-73.3	2018	2019	10	https://doi.org/10.17190/AMF/1671889
BR-Npw	FLUXNET	-16.5	-56.4	2013	2016	30	https://doi.org/10.18140/FLX/1669368
BW-Gum	C. Helfter	-19	22.4	2018	2020	26	https://doi.org/10.5285/d366ed40-af8c-42be-86f2-bb90b11a659e
BW-Nxr	C. Helfter	-19.5	23.2	2018	2020	12	https://doi.org/10.5285/2170ebd0-7e6f-4871-97d9-1d42e210468f
NZ-Kop	FLUXNET	-37.4	175.6	2012	2015	48	https://doi.org/10.18140/FLX/1669652

B   Monthly measurement fit
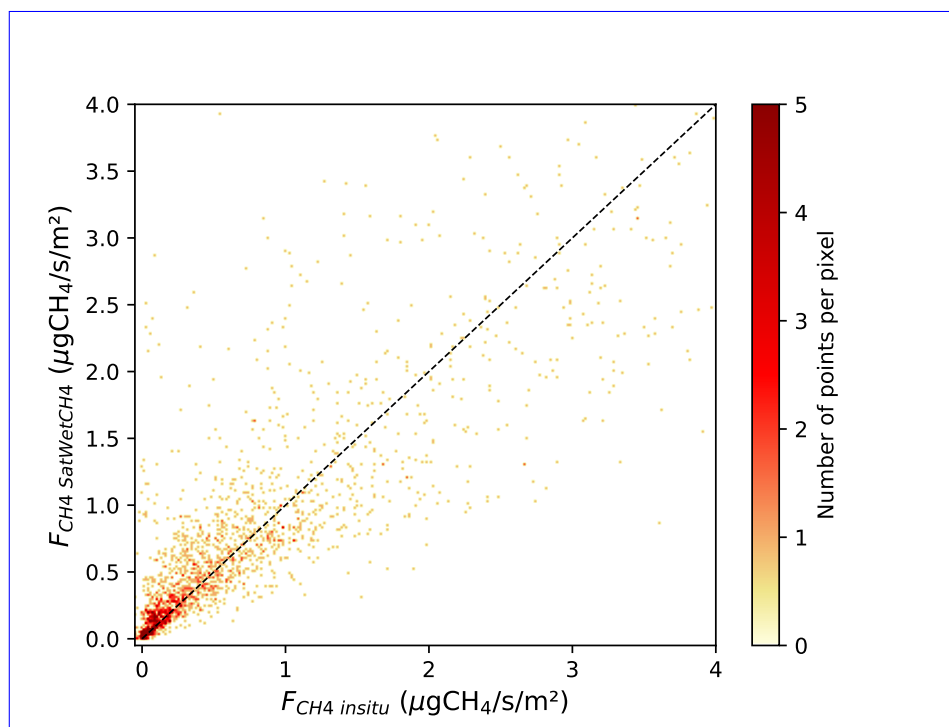
Figure S1. SatWetCH4 monthly modelled fluxes in function of the monthly in situ measurement, with the 1:1 dashed line.

C Comparison of ERA5 data with in situ data

C.1 Temperature

We study the variable *Soil temperature level 2 (lay2)* from ERA5, which represents soil temperature in 7-28 cm soil layer. We compare it to soil temperature measurements available at the sites. Out of the 58 sites, 42 are equipped with temperature probes. If multiple probes are available, we choose the one closest to the surface. For ERA5, we select the nearest pixel to the site.

ERA5 *lay2* temperature is consistent with in situ measurements. The comparison is shown in Fig.S2. Each site is represented by a point. In Fig.S2.a., the temporal correlation between ERA5 temperature and observations is strong: r is bigger than 0.9 for 37 out of 42 sites. A RMSD lower than 2 °K is shown for 39 out of 42 sites on Fig.S2.b. ERA5 temperatures have a good spatial correlation on average with observations, as Fig.S2.c. shows a linear relationship between mean in situ temperatures and mean ERA5 *lay2* temperatures. There is an RMSD of 1.8 °K between the observation and ERA5 means. Finally, Fig.S2.d. indicates a good reproduction of the seasonal variations for ERA5 *lay2*: the RMSD between the sites standard deviations of observations and ERA5 is 1.2 °K.
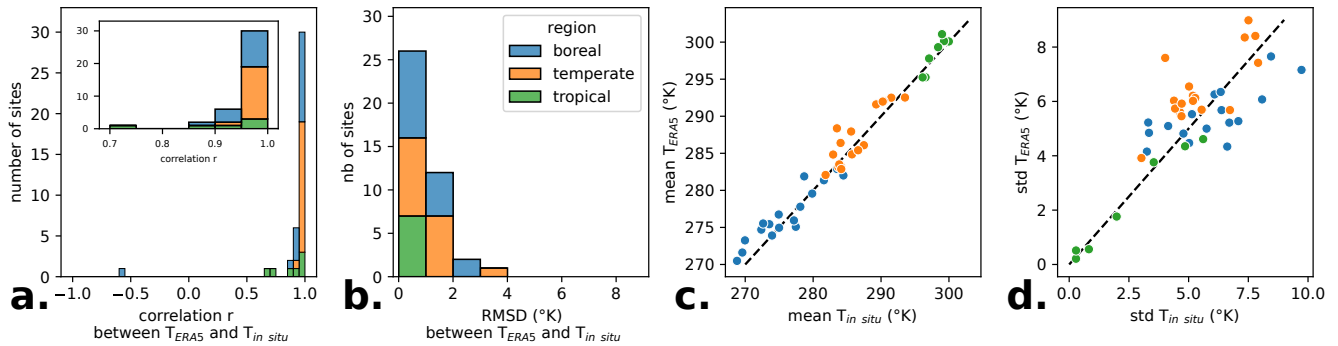
Figure S2. Comparison of 0.25° ERA5 *lay2* temperature with in situ temperature measurements. ERA5 data consistently match local in situ measurements. ~~Each point represents a site.~~ **a.** Temporal correlation coefficient between ERA5 *lay2* temperature and in situ data. **b.** RMSD of ERA5 data compared to observations. **c.** Spatial pattern: mean in situ temperature for each site compared to mean of ERA5 estimates. **d.** Amplitude comparison: standard deviation of in situ temperature for each site compared to standard deviation of ERA5 estimates. In c. and d., each point represents a site.

C.2 Soil Water Content (SWC)

We study the variable *SWC level 2* from ERA5, which represents Soil Water Content (SWC) in 7-28 cm soil layer. We compare it to SWC measurements available at the sites. Out of the 58 sites, 14 are equipped with SWC probes. For ERA5, we select the nearest pixel to the site.

20   ERA5 SWC 0.25° data do not consistently match local in situ measurements. Indeed, Fig.S3.a. shows an unclear temporal correlation between in situ SWC and ERA5 SWC. Fig.S3.b. indicates high RMSDs (0-30% for values around 40%) between ERA5 and local SWC measurements. Moreover, ERA5 tends to underestimate the mean SWC compared to local measurements as shown in Fig.S3.c. ERA5 highlights a significant underestimation of SWC variation amplitude by ERA5 compared to observations (Fig.S3.d.).
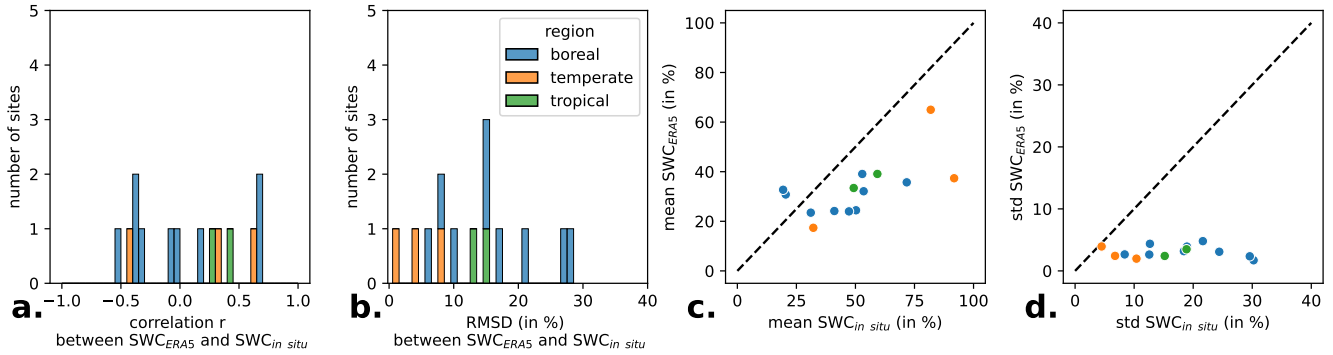
Figure S3. Comparison of 0.25° *lay2* ERA5 Soil Water Content (SWC) with local in situ SWC observations. ERA5 data does not consistently match local in situ measurements. Each point represents a site. **a.** Temporal correlation between in situ SWC and ERA5 SWC. **b.** RMSD between ERA5 SWC and observed local SWC. **c.** Spatial pattern: mean in situ SWC for each site compared to mean of ERA5 SWC. **d.** Amplitude comparison: standard deviation of in situ SWC for each site compared to standard deviation of ERA5 estimates.
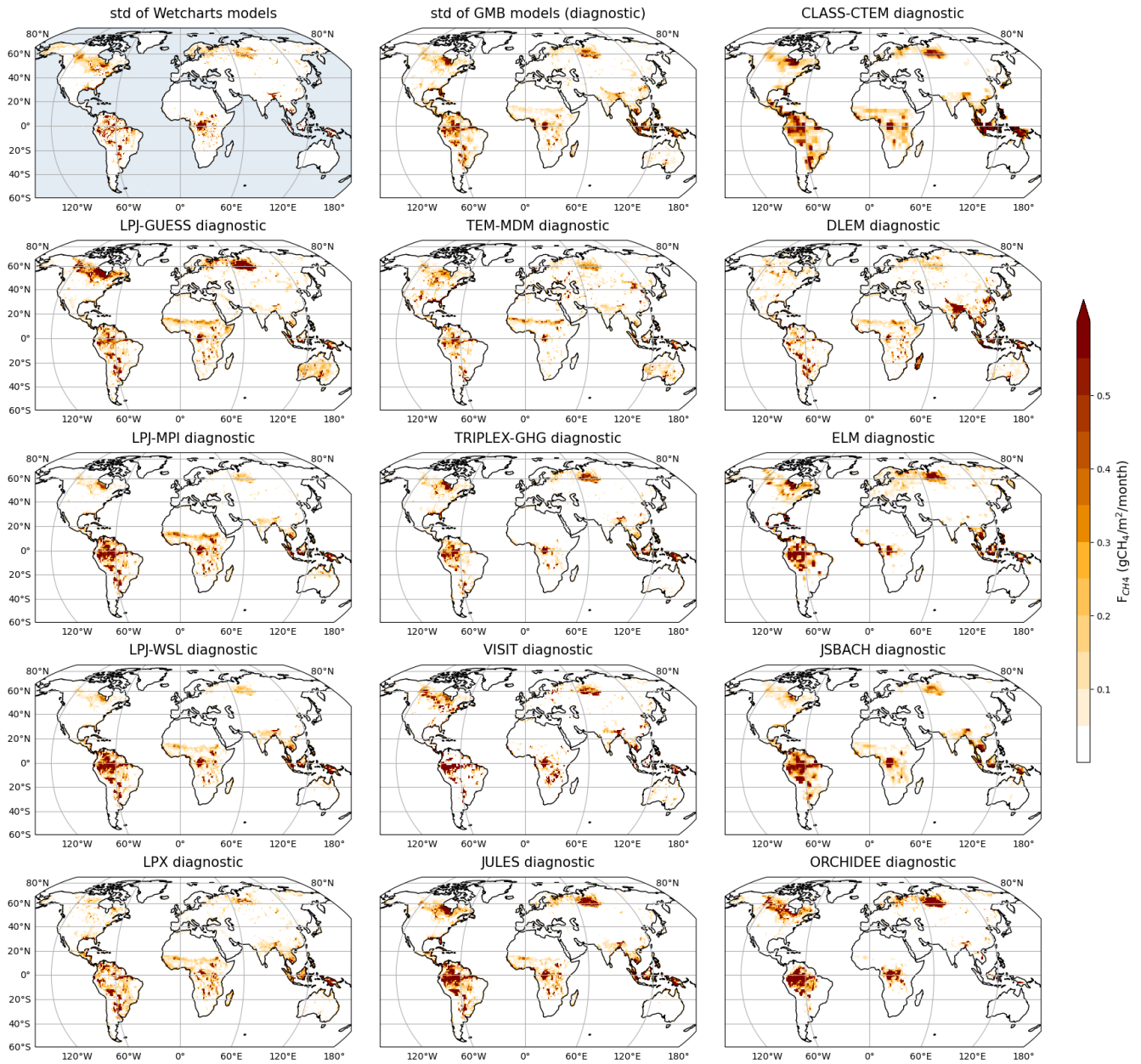
Figure S4. Emissions monthly mean for 2003-2018 of Land surface Models run with WAD2M for GMB (Saunois et al., 2020). Spatial patterns and intensity show considerable variability between the different GMB Land Surface Models, especially in Canada, subequatorial Africa, Siberian Lowland, and Australia.
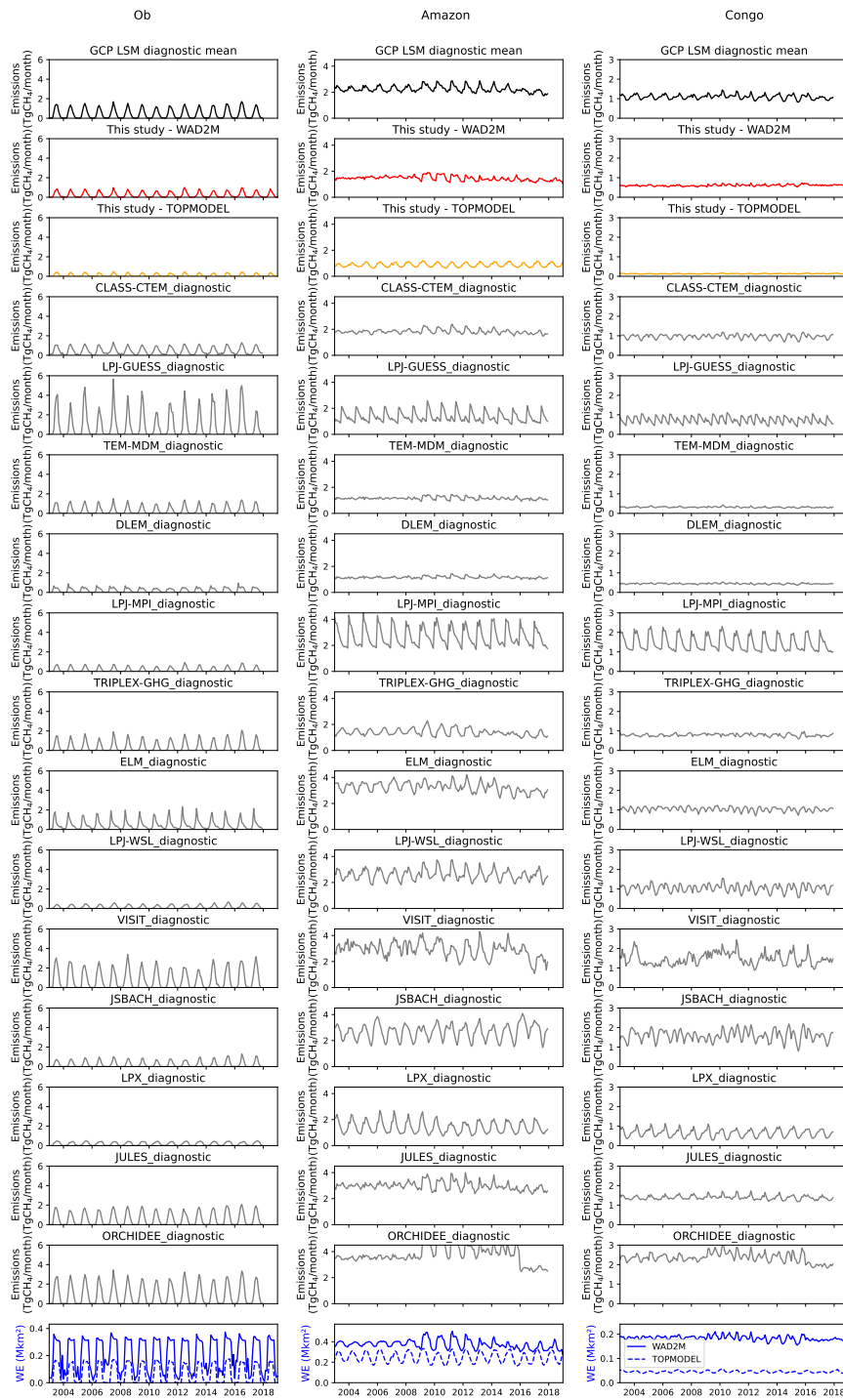
Figure S5. Methane emissions from different basins (Ob, Amazon and Congo) from the mean of the GMB LSM models diagnostic (black), our simulations (red), and each LSM from GMB diagnostic runs (grey). The Wetland Extent (WE) used for the runs is WAD2M and is shown in the lower graphs.

References

Saunois, M., Stavert, A. R., Poulter, B., Bousquet, P., Canadell, J. G., Jackson, R. B., Raymond, P. A., Dlugokencky, E. J., Houweling, S., Patra, P. K., Ciais, P., Arora, V. K., Bastviken, D., Bergamaschi, P., Blake, D. R., Brailsford, G., Bruhwiler, L., Carlson, K. M., Carrol, M., Castaldi, S., Chandra, N., Crevoisier, C., Crill, P. M., Covey, K., Curry, C. L., Etiope, G., Frankenberg, C., Gedney, N., Hegglin, M. I., Höglund-Isaksson, L., Hugelius, G., Ishizawa, M., Ito, A., Janssens-Maenhout, G., Jensen, K. M., Joos, F., Kleinen, T., Krummel, P. B., Langenfelds, R. L., Laruelle, G. G., Liu, L., Machida, T., Maksyutov, S., McDonald, K. C., McNorton, J., Miller, P. A., Melton, J. R., Morino, I., Müller, J., Murguia-Flores, F., Naik, V., Niwa, Y., Noce, S., O'Doherty, S., Parker, R. J., Peng, C., Peng, S., Peters, G. P., Prigent, C., Prinn, R., Ramonet, M., Regnier, P., Riley, W. J., Rosentreter, J. A., Segers, A., Simpson, I. J., Shi, H., Smith, S. J., Steele, L. P., Thornton, B. F., Tian, H., Tohjima, Y., Tubiello, F. N., Tsuruta, A., Viovy, N., Voulgarakis, A., Weber, T. S., van Weele, M., van der Werf, G. R., Weiss, R. F., Worthy, D., Wunch, D., Yin, Y., Yoshida, Y., Zhang, W., Zhang, Z., Zhao, Y., Zheng, B., Zhu, Q., Zhu, Q., and Zhuang, Q.: The Global Methane Budget 2000–2017, Earth System Science Data, 12, 1561–1623, https://doi.org/10.5194/essd-12-1561-2020, 2020.